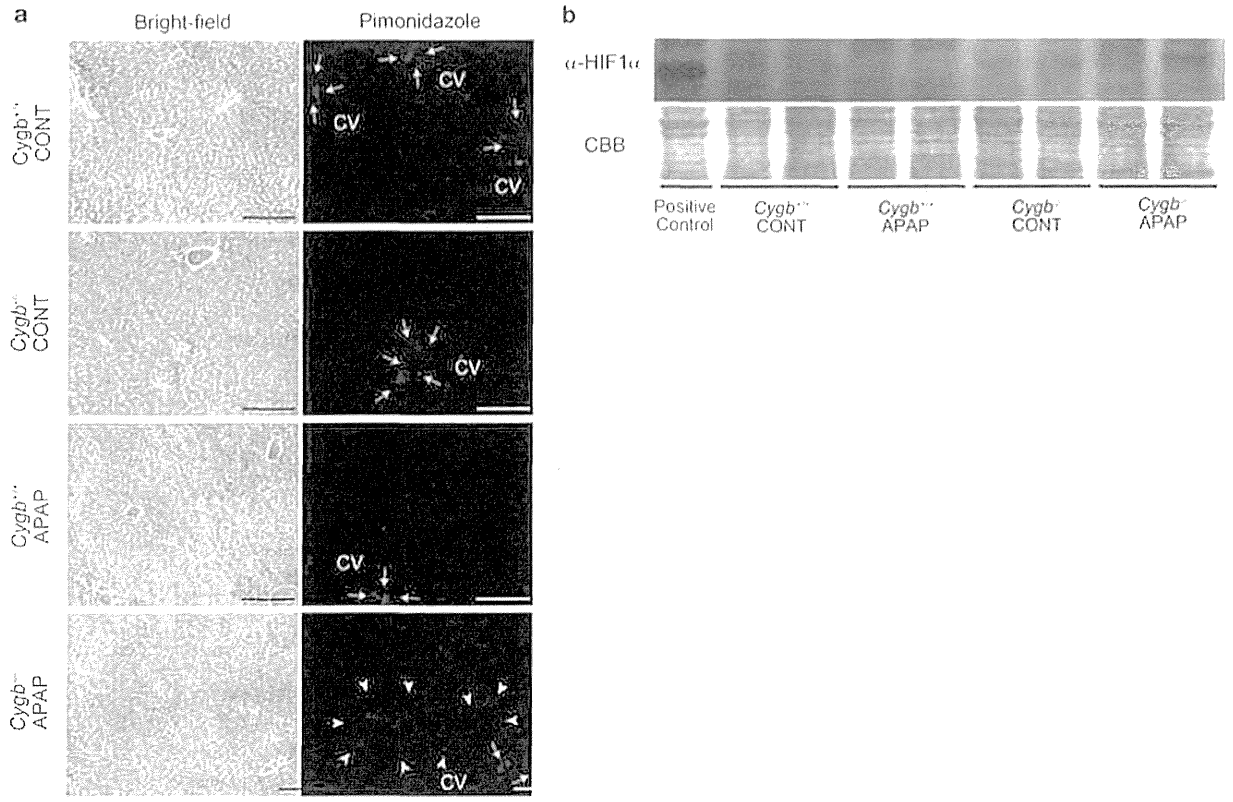

Figure 3 Determination of hypoxic conditions in mouse liver. (**a**) Pimonidazole staining in the livers of *cytoglobin* (*Cygb*)$^{+/+}$ (left) and *Cygb*$^{-/-}$ (right) mice 6 h after APAP treatment. Arrowheads indicate pimonidazole-positive areas. Arrows indicate the central vein (CV) ($\times$ 100, bar = 200 μm). (**b**) Western blotting of hypoxia-inducible factor 1α (HIF-1α) protein. Coomassie brilliant blue (CBB) staining was used for the normalization.

Deterioration of the Viability of Primary-Cultured Mouse Hepatocytes by Co-Culture With HSCs Under APAP Treatment

Next, we studied whether the presence of HSCs influences the viability of mouse hepatocytes under conditions of APAP treatment. No difference in cell viability following APAP challenge was observed between wild-type and *Cygb*-null hepatocytes in monoculture under 5% O_2 (Figure 5a). However, hepatocytes co-cultured with wild-type HSCs showed significantly lower cell viability after APAP challenge compared with those co-cultured with *Cygb*-null HSCs: the cell viability values of hepatocytes in monoculture, those co-cultured with wild-type HSCs, and those co-cultured with *Cygb*-null HSCs were 0.29, 0.20, and 0.32, respectively (Figure 5b). In addition, hepatocytes showed a similar sensitivity to APAP when conditioned media from wild-type and *Cygb*-null HSCs were applied (Figure 5c). These results support the hypothesis that HSC-CYGB influences the behavior of hepatocytes, presumably through the O_2 supply.

Alleviation of CCL_4-Induced, but Not LPS/D-GalN-Induced, Acute Liver Injury By CYGB Deficiency

To investigate whether the mitigation of hepatocyte damage is unique to APAP in *Cygb*-null mice, two other acute liver injury models, ie, CCl_4-induced and LPS/D-GalN-induced liver damage, were employed. CCl_4 is metabolized by CYP2E1, similar to APAP. In contrast, LPS-induced liver injury is generally associated with Toll-like receptor 4 signaling pathways and is independent of CYP activity. In the CCl_4 model, the serum ALT levels were significantly higher in the wild-type mice (14 800 $\pm$ 1500 U/l) than in the *Cygb*-null mice (4340 $\pm$ 1030 U/l), similar to the APAP model (Figure 6a). The histologic analysis revealed that centrilobular necrosis was more severe in the wild-type mice than in the *Cygb*-null mice (Figure 6b). In contrast, in the LPS/D-GalN model the serum ALT levels of the wild-type mice did not differ from those of the *Cygb*-null mice (333 $\pm$ 116 and 402 $\pm$ 189 U/l, respectively) (Figure 6c). A pathological analysis revealed the degeneration and necrosis of hepatocytes, the destruction of the hepatic architecture, and the presence of hemorrhage in both mouse strains (Figure 6d). These data support the hypothesis that CYGB deficiency decelerates the CYP2E1-mediated xenobiotic toxicity in the liver.

DISCUSSION

The current study demonstrated that APAP-induced liver injury was attenuated in *Cygb*-null mice compared with wild-type mice. CCl_4-induced liver injury was also alleviated in

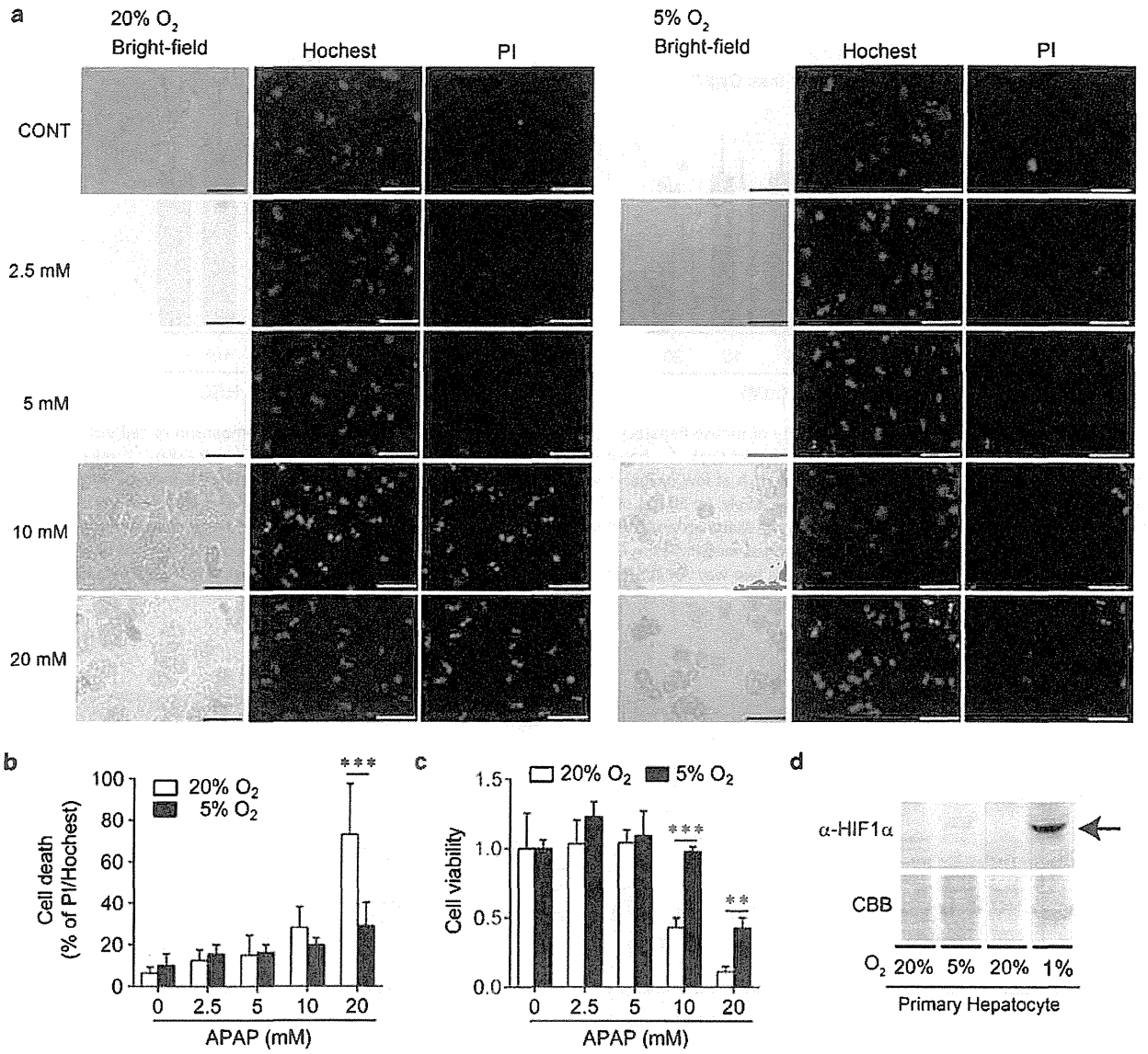

Figure 4 Influence of oxygen level on *N*-acetyl-*p*-aminophenol (APAP)-induced hepatocyte injury in culture. (**a**) Representative images of APAP-induced hepatocyte damage. Cell death was determined using propidium iodide (PI) staining under 5 or 20% oxygen (O_2) 16 h after APAP administration. The concentrations of APAP were 0, 2.5, 5, 10, and 20 mM. Stained hepatocytes were observed under bright-field (left) and dark-field microscopy (center, Hoechst 33342; right, PI; × 400, bar = 50 μm). (**b**) Determination of cell death calculated as the ratio of PI-positive hepatocytes under 5 or 20% O_2. The values represent the percentage ratio of PI-positive hepatocytes to Hoechst-positive hepatocytes ($n = 4$–8). (**c**) Determination of cell viability by an MTT assay. Significance was determined by a two-way ANOVA with Bonferroni's test (**b** and **c**). $^{**}P < 0.01$, $^{***}P < 0.001$. (**d**) Western blotting of HIF-1α protein under conditions of 1, 5, and 20% O_2. Arrow indicated HIF-1α protein. Coomassie brilliant blue (CBB) staining was used for the normalization.

Cygb-null mice. APAP and CCl_4 toxicity is mediated through the production of reactive metabolites by CYP2E1. The hepatic CYP2E1 expression levels and in the *Cygb*-null mice were similar to those of the wild-type mice; nevertheless, the serum levels of NAPQI derivatives, such as cysteinyl-APAP and *N*-acetyl-cysteinyl-APAP, were lower in the *Cygb*-null mice than in the wild-type mice under APAP challenge. In addition, the serum APAP levels were elevated, albeit not significantly, in the *Cygb*-null mice compared with the wild-type mice. These results suggest that the generation of NAPQI is reduced in *Cygb*-null mice in the absence of changes in the hepatic CYP2E1 protein levels, and they support the theory that the enzymatic activity of CYP2E1 is attenuated in *Cygb*-null mice.

In this study, the hepatic microsomal CYP2E1 activity (under condition of disrupted sinusoidal microenvironment) in the *Cygb*-null mice was similar to that in the wild-type mice (Figure 2c). Considering that (1) CYPs are mono-

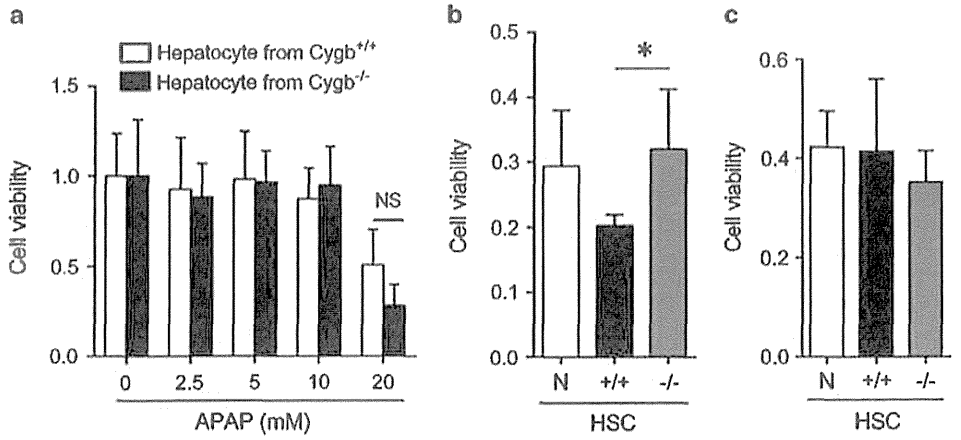

Figure 5 Presence of HSCs deteriorates the viability of mouse hepatocytes under conditions of APAP treatment. (**a**) Comparison of cell viability 16 h after APAP challenge between cytoglobin (*Cygb*)$^{+/+}$ and *Cygb*$^{-/-}$ hepatocytes. (**b**) Effect of HSCs isolated from *Cygb*$^{+/+}$ or *Cygb*$^{-/-}$ mice on hepatocyte viability after 30 mM APAP challenge for 16 h at low oxygen level (5% oxygen (O_2)). White, black, and gray columns indicate without HSCs, with *Cygb*$^{+/+}$ HSCs, and with *Cygb*$^{-/-}$ HSCs, respectively. (**c**) Effects of HSC-conditioned media on hepatocyte viability after 30 mM APAP challenge. Conditioned media were prepared as described in the Materials and Methods section. White, black, and gray columns indicate culture in the absence of conditioned medium, in the presence of conditioned medium from *Cygb*$^{+/+}$ HSCs, and in the presence of conditioned medium from *Cygb*$^{-/-}$ HSCs, respectively. Significance was determined by a two-way ANOVA with Bonferroni's test (**a**) and a one-way ANOVA with Bonferroni's test (**b** and **c**). $^{*}P<0.05$; NS, not significant.

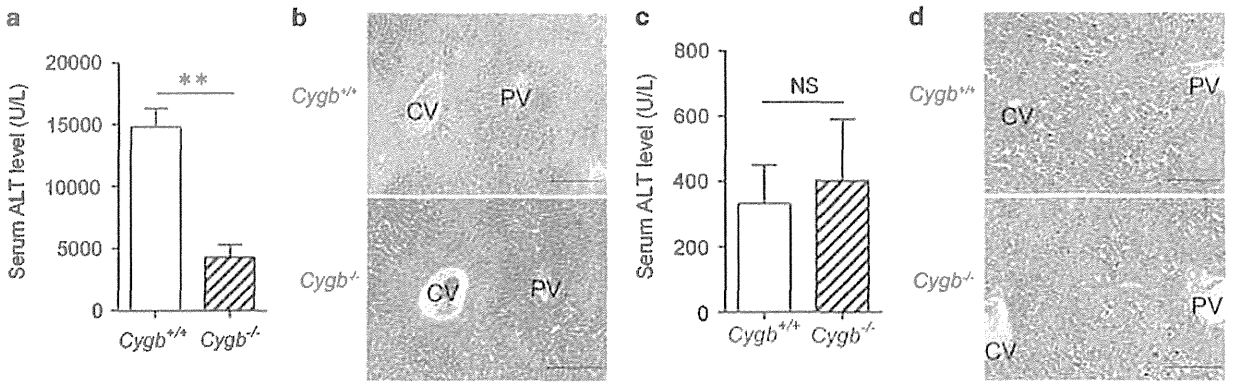

Figure 6 Carbon tetrachloride (CCl_4)-induced and lipopolysaccharide (LPS)/D-galactosamine (D-GalN)-induced acute liver injury in mice. (**a** and **b**) Acute liver injury induced by 0.5 mg/kg CCl_4 administration. Serum alanine aminotransferase (ALT) activity (**a**) and liver histology (**b**; × 200, bar = 100 μm) 24 h after CCl_4 injection are shown (each, $n = 3$–4). CV, central vein; PV, portal vein. (**c** and **d**) Acute liver injury induced by 700 mg/kg of D-GalN and 5 μg/kg of LPS. Serum ALT activity (**c**) and liver histology (**d**; × 200, bar = 100 μm) 6 h after LPS/D-GalN injection are shown (each, $n = 10$). CV, central vein; PV, portal vein. Significance was determined by an unpaired *t*-test ($^{**}P<0.01$; NS, not significant).

oxygenases and (2) CYGB functions as an O_2-binding protein, we concluded that the APAP-derived toxicity may differ with regard to hepatic O_2 levels between *Cygb*-null and wild-type mice. In addition, pimonidazole-positive areas, indicating hypoxic conditions, were expanded only in the *Cygb*-null mice, although HIF1α activation was not detected. As well as our observation, it has been reported that pimonidazole-positive cells are not always identical to HIF1α-activated cells.[20,21] Thus, we considered that the *Cygb*-null mice exhibited low O_2 tension in the liver, particularly after APAP challenge. Yan *et al.*[5] showed that APAP-induced cell death in cultured mouse hepatocytes was attenuated in the presence of 10% O_2, which was accompanied by a decrease in mitochondrial oxidative stress. In the present study, we also observed that APAP-induced toxicity in mouse primary hepatocytes was alleviated even at lower O_2 levels (5% O_2). Surprisingly, co-culture with wild-type HSCs, but not with *Cygb*-null HSCs, exacerbated the APAP-induced hepatocyte death under a 5% O_2 atmosphere. In addition, conditioned media from wild-type HSCs and from *Cygb*-null HSCs failed to influence the APAP-induced hepatocyte death, indicating that stable components in these conditioned media, such as proteins and lipids, were ineffective. Although the co-culture system used in this study can't be said to reproduce perfectly

the sinusoidal environment *in vivo*, these results indicate that the HSC-CYGB could affect APAP-induced hepatocyte injury.

The O_2 affinity of CYGB has been reported to be equivalent to that of myoglobin and neuroglobin, and is considerably higher than that of hemoglobin.[6] This fact suggests that CYGB releases O_2 at lower O_2 tension compared with hemoglobin and, in combination, (1) HIF1α protein was detected in the hepatocytes cultured with 1% O_2 but not in that with 20 and 5% O_2; (2) in fact, the wild-type HSCs, but not *Cygb*-null HSCs, can accelerate the APAP hepatocyte injury under 5% O_2; CYGB may be an early sensor for low oxygen level and supply O_2 to neighboring cells before falling in hypoxia (activation of HIF). In other words, CYGB can have a role in O_2 supply after the consumption of O_2 derived from hemoglobin *in vivo*. When excess CYP2E1 metabolism causes a shortage of O_2 in hepatocytes, the HSC–CYGB may supply O_2 temporarily and locally to hepatocytes during the O_2 insufficiency.

It has been reported that APAP damages the hepatic microvasculature, which precedes hepatocellular injury. *In vivo* microscopy indicated that this damage consists of endothelial cell swelling and the penetration of erythrocytes into the space of Disse. Significant decreases in the blood supply in hepatic sinusoids were observed 2 and 6 h after APAP administration.[22] In contrast, when HSCs become activated, they undergo changes in the cytoskeletal machinery and gain the ability to contract.[23] Some studies have demonstrated that activated HSCs contract in response to various agents.[24,25] Thus, activated HSCs are thought to be involved in the disturbance of hepatic microcirculation.[26] A previous study reported that CYGB was able to suppress HSC activation.[27] Considering all of these reports, the loss of CYGB may lead to the 'priming' of HSCs to the activated stage and can cause immediate sinusoidal constriction after APAP challenge due to HSC contraction. However, the hypothesis could be denied, because *Cygb*-null mice did not show attenuated LPS-induced liver injury.

In conclusion, the present study demonstrated in part that APAP-induced acute liver injury was attenuated in *Cygb*-null mice, presumably due to local low O_2 level (but not hypoxia) around hepatocytes closely adherent to HSCs (Figure 7). Although the molecular mechanism of O_2 transfer from HSCs to hepatocytes remains uncharacterized, this study

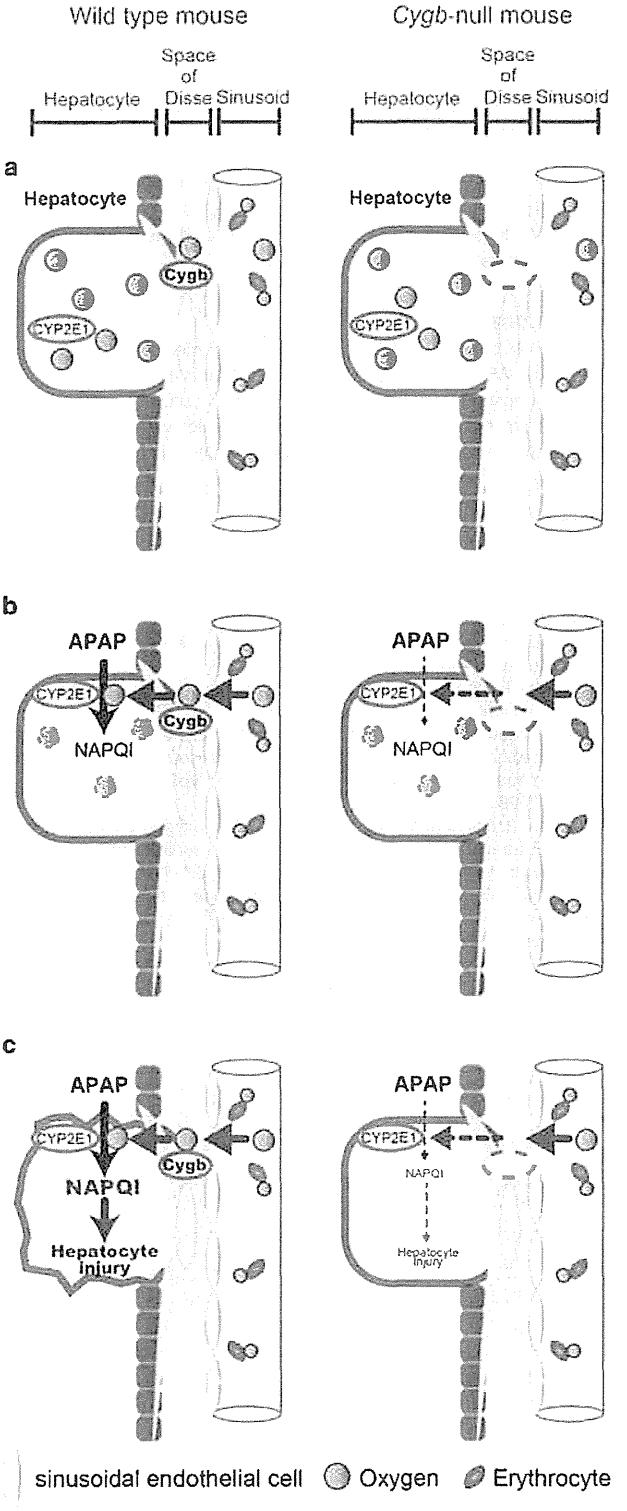

Figure 7 Putative mechanism by which hepatic stellate cell (HSC)-expressed cytoglobin (CYGB) is involved in *N*-acetyl-*p*-aminophenol (APAP)-induced liver injury. (**a**) The oxygen (O_2) concentration in the livers of *Cygb*-null mice was similar to that of wild-type mice under normal conditions. (**b**) At high APAP concentrations, APAP is metabolized by CYP2E1 and O_2 is rapidly consumed. As a result, hepatocytes tend to be temporarily O_2 deficient. O_2 would be supplied from CYGB in HSCs located in the space of Disse in wild-type mice, but this is not the case in *Cygb*-null mice. (**c**) Thus, CYP2E1 efficiently generates *N*-acetyl-*p*-benzoquinone imine (NAPQI) from APAP in wild-type mice. In contrast, in *Cygb*-null mice NAPQI production is decreased because of impaired local O_2 supply from HSCs; thus, NAPQI-dependent hepatocyte injury is attenuated. Blue arrows indicate O_2 transfer. Bold black arrows indicate the pathway by which APAP toxicity is mediated. Dashed line arrows indicate reduction.

provides important evidence to further understand the molecular mechanism of drug-induced liver injury mediated by CYP2E1.

Supplementary Information accompanies the paper on the Laboratory Investigation website (http://www.laboratoryinvestigation.org)

ACKNOWLEDGMENTS

We thank Ms Chiho Kadono for animal care, and Dr Wenhao Cui, Dr Keiko Iwaisako, and Dr Kazuki Nakatani (Osaka City University) for their valuable discussion and comments on this study. This investigation was supported in part by a Grant-in-Aid for Scientific Research (B) from the Japan Society for the Promotion of Science (JSPS) through grant 25293177 (to NK) (2013–2016), the Mochida Memorial Foundation (to TM), and the National Cancer Institute Intramural Research Program (to FJG).

AUTHOR CONTRIBUTIONS

YT, TM, and NK conceived and designed the experiments. KWK and FJG quantified the APAP metabolites. LT provided technical assistance in the isolation of hepatocytes and HSCs. KI and KY contributed critically to the design of the manuscript in terms of important intellectual content. YT, TM, and NK wrote the manuscript, with suggestions from all authors.

DISCLOSURE/CONFLICT OF INTEREST

The authors declare no conflict of interest.

1. Lieber CS. Cytochrome P-4502E1: its physiological and pathological role. Physiol Rev 1997;77:517–544.
2. Gonzalez FJ. The 2006 Bernard B. Brodie Award Lecture. Cyp2e1. Drug Metab Dispos 2007;35:1–8.
3. Gonzalez FJ, Kimura S. Study of P450 function using gene knockout and transgenic mice. Arch Biochem Biophys 2003;409:153–158.
4. Chen C, Krausz KW, Idle JR, *et al.* Identification of novel toxicity-associated metabolites by metabolomics and mass isotopomer analysis of acetaminophen metabolism in wild-type and Cyp2e1-null mice. J Biol Chem 2008;283:4543–4559.
5. Yan HM, Ramachandran A, Bajt ML, *et al.* The oxygen tension modulates acetaminophen-induced mitochondrial oxidant stress and cell injury in cultured hepatocytes. Toxicol Sci 2010;117:515–523.
6. Hankeln T, Ebner B, Fuchs C, *et al.* Neuroglobin and cytoglobin in search of their role in the vertebrate globin family. J Inorg Biochem 2005;99:110–119.
7. Tosqui P, Colombo MF. Neuroglobin and cytoglobin: two new members of globin family. Rev Bras Hematol Hemoter 2011;33:307–311.
8. Avivi A, Gerlach F, Joel A, *et al.* Neuroglobin, cytoglobin, and myoglobin contribute to hypoxia adaptation of the subterranean mole rat Spalax. Proc Natl Acad Sci USA 2010;107:21570–21575.
9. Nakatani K, Okuyama H, Shimahara Y, *et al.* Cytoglobin/STAP, its unique localization in splanchnic fibroblast-like cells and function in organ fibrogenesis. Lab Invest 2004;84:91–101.
10. Schmidt M, Gerlach F, Avivi A, *et al.* Cytoglobin is a respiratory protein in connective tissue and neurons, which is up-regulated by hypoxia. J Biol Chem 2004;279:8063–8069.
11. Oleksiewicz U, Liloglou T, Field JK, *et al.* Cytoglobin: biochemical, functional and clinical perspective of the newest member of the globin family. Cell Mol Life Sci 2011;68:3869–3883.
12. Kawada N, Kristensen DB, Asahina K, *et al.* Characterization of a stellate cell activation-associated protein (STAP) with peroxidase activity found in rat hepatic stellate cells. J Biol Chem 2001;276:25318–25323.
13. Mabuchi A, Mullaney I, Sheard PW, *et al.* Role of hepatic stellate cell/hepatocyte interaction and activation of hepatic stellate cells in the early phase of liver regeneration in the rat. J Hepatol 2004;40:910–916.
14. Yin C, Evason KJ, Asahina K, *et al.* Hepatic stellate cells in liver development, regeneration, and cancer. J Clin Invest 2013;123:1902–1910.
15. Thuy le TT, Morita T, Yoshida K, *et al.* Promotion of liver and lung tumorigenesis in DEN-treated cytoglobin-deficient mice. Am J Pathol 2011;179:1050–1060.
16. Iwaisako K, Hatano E, Taura K, *et al.* Loss of Sept4 exacerbates liver fibrosis through the dysregulation of hepatic stellate cells. J Hepatol 2008;49:768–778.
17. da Rosa EJ, da Silva MH, Carvalho NR, *et al.* Reduction of acute hepatic damage induced by acetaminophen after treatment with diphenyl diselenide in mice. Toxicol Pathol 2012;40:605–613.
18. Ishibe T, Kimura A, Ishida Y, *et al.* Reduced acetaminophen-induced liver injury in mice by genetic disruption of IL-1 receptor antagonist. Lab Invest 2009;89:68–79.
19. Samoszuk MK, Walter J, Mechetner E. Improved immunohistochemical method for detecting hypoxia gradients in mouse tissues and tumors. J Histochem Cytochem 2004;52:837–839.
20. Harada H, Inoue M, Itasaka S, *et al.* Corrigendum: Cancer cells that survive radiation therapy acquire HIF-1 activity and translocate toward tumour blood vessels. Nat Commun 2013;4:2314.
21. Tanaka H, Yamamoto M, Hashimoto N, *et al.* Hypoxia-independent overexpression of hypoxia-inducible factor 1alpha as an early change in mouse hepatocarcinogenesis. Cancer Res 2006;66:11263–11270.
22. Hinson JA, Roberts DW, James LP. Mechanisms of acetaminophen-induced liver necrosis. Handb Exp Pharmacol 2010369–405.
23. Jiang JX, Torok NJ. Liver Injury and the Activation of the Hepatic Myofibroblasts. Curr Pathobiol Rep 2013;1:215–223.
24. Friedman SL. Hepatic stellate cells: protean, multifunctional, and enigmatic cells of the liver. Physiol Rev 2008;88:125–172.
25. Reynaert H, Thompson MG, Thomas T, *et al.* Hepatic stellate cells: role in microcirculation and pathophysiology of portal hypertension. Gut 2002;50:571–581.
26. Vollmar B, Menger MD. The hepatic microcirculation: mechanistic contributions and therapeutic targets in liver injury and repair. Physiol Rev 2009;89:1269–1339.
27. Cui W, Wang M, Maegawa H, *et al.* Inhibition of the activation of hepatic stellate cells by arundic acid via the induction of cytoglobin. Biochem Biophys Res Commun 2012;425:642–648.

The American Journal of Pathology, Vol. 185, No. 4, April 2015

The American Journal of
PATHOLOGY
ajp.amjpathol.org

GASTROINTESTINAL, HEPATOBILIARY, AND PANCREATIC PATHOLOGY

Cytoglobin Deficiency Promotes Liver Cancer Development from Hepatosteatosis through Activation of the Oxidative Stress Pathway

Le Thi Thanh Thuy,* Yoshinari Matsumoto,*† Tuong Thi Van Thuy,* Hoang Hai,* Maito Suoh,‡ Yuka Urahara,* Hiroyuki Motoyama,* Hideki Fujii,* Akihiro Tamori,* Shoji Kubo,§ Shigekazu Takemura,§ Takashi Morita,¶ Katsutoshi Yoshizato,*‖ and Norifumi Kawada*

From the Departments of Hepatology, Medical Education and General Practice,‡ Hepato-Biliary-Pancreatic Surgery,§ and Molecular Genetics,¶ Graduate School of Medicine, and the Department of Medical Nutrition,† Graduate School of Human Life Science, Osaka City University, Osaka; and the PhoenixBio Co. Ltd.,‖ Hiroshima, Japan*

Accepted for publication
December 11, 2014.

Address correspondence to Norifumi Kawada, M.D., Ph.D., Department of Hepatology, Graduate School of Medicine, Osaka City University, 1-4-3 Asahimachi, Abeno, Osaka 545-8585, Japan. E-mail: kawadanori@med.osaka-cu.ac.jp.

This study was conducted to clarify the role of cytoglobin (Cygb), a globin expressed in hepatic stellate cells (HSCs), in the development of liver fibrosis and cancer in nonalcoholic steatohepatitis (NASH). Cygb expression was assessed in patients with NASH and hepatocellular carcinoma. Mouse NASH model was generated in *Cygb*-deficient ($Cygb^{-/-}$) or wild-type (WT) mice by giving a choline-deficient amino acid–defined diet and, in some of them, macrophage deletion and N-acetyl cysteine treatment were used. Primary-cultured mouse HSCs isolated from WT ($HSCs^{Cygb-wild}$) or $Cygb^{-/-}$ ($HSCs^{Cygb-null}$) mice were characterized. As results, the expression of CYGB was reduced in patients with NASH and hepatocellular carcinoma. Choline-deficient amino acid treatment for 8 weeks induced prominent inflammation and fibrosis in $Cygb^{-/-}$ mice, which was inhibited by macrophage deletion. Surprisingly, at 32 weeks, despite no tumor formation in the WT mice, all $Cygb^{-/-}$ mice developed liver cancer, which was ameliorated by N-acetyl cysteine treatment. Altered expression of 31 genes involved in the metabolism of reactive oxygen species was notable in $Cygb^{-/-}$ mice. Both $HSCs^{Cygb-null}$ and *Cygb* siRNA-transfected-$HSCs^{Cygb-wild}$ exhibited the preactivation condition. Our findings provide important insights into the role that *Cygb*, expressed in HSCs during liver fibrosis, plays in cancer development with NASH. *(Am J Pathol 2015, 185: 1045–1060; http://dx.doi.org/10.1016/j.ajpath.2014.12.017)*

Nonalcoholic steatohepatitis (NASH), an increasingly recognized obesity-related liver disease, is characterized by hepatocyte steatosis accompanied by a fibroinflammatory reaction.[1,2] Several studies have shown that NASH patients are at risk for progression to cirrhosis, the most common risk factor for hepatocellular carcinoma (HCC).[1,3] Compared to what is known about the pathogenesis of hepatitis virus–induced HCC, insight into NASH-associated HCC remains immature.

Currently, it is thought that the liver develops NASH via several pathological steps. Hepatocytes undergo degeneration characterized by the accumulation of fatty acids, which are excessively oxidized in the cellular organelles, including mitochondria. During this process, reactive oxygen species (ROS) are produced and trigger oxidative stress, leading to cell and tissue damage.[1] Hepatic macrophages consisting of resident Kupffer cells and infiltrating bone marrow–derived macrophages produce inflammatory mediators, such as tumor necrosis factor α (TNF-α), IL-6, IL-1β, and ROS.[4,5] These mediators further stimulate hepatocyte steatosis and initiate the activation of hepatic stellate cells (HSCs). Finally, the persistent secretion of ROS and mediators from these cells induces the development of advanced fibrosis.

Supported by Japan Society for the Promotion of Science (JSPS) Grant-in-Aid for Young Scientific Research grant 25860554 (L.T.T.T.); JSPS Grant-in-Aid for Scientific Research grants 21390232 (N.K.), 23112518 (N.K.), and 25293177 (N.K.); and Research on Hepatitis and BSE, the Ministry of Health Labor and Welfare (N.K.).

Disclosures: None declared.

http://dx.doi.org/10.1016/j.ajpath.2014.12.017

Cytoglobin (Cygb) was originally discovered in rat HSCs in 2001,[6] and is the fourth globin to be discovered in mammals.[7,8] CYGB is present in fibroblasts that store vitamin A in the visceral organs, including the liver and pancreas.[9] CYGB facilitates oxygen (O_2) diffusion through tissues, scavenges nitric oxide (NO) and other ROS, has a protective function during oxidative stress,[10] and suppresses tumorigenesis.[11–14] We previously showed that *Cygb*-deficient ($Cygb^{-/-}$) mice exhibit susceptibility to cancer development in the liver and lung with diethylnitrosamine administration.[15] Therefore, the absence of CYGB likely promotes a carcinogenic process in the presence of liver disease.

The present study clarifies the role of *Cygb* in steatohepatitis induced by a choline-deficient amino acid–defined diet (CDAA) in mice. The CDAA diet is a useful model to investigate NASH because it induces fibrosis, systemic insulin resistance, and steatohepatitis, which are compatible to the pathophysiology of human NASH. The administration of CDAA to C57BL/6 wild-type (WT) mice was reported to induce defined liver fibrosis not earlier than 22 weeks, and HCC nodules at a late time point, 84 weeks.[16] Herein, we showed $Cygb^{-/-}$ mice fed a CDAA diet, leading to a severe NASH condition and a 100% incidence of HCC at an early time point, 32 weeks. Moreover, primary untreated HSCs isolated from $Cygb^{-/-}$ mice showed a preactivated condition characterized by augmented ROS and cytokine production.

Materials and Methods

Human Tissues and Specimens

Human NASH specimens ($n = 15$), used for immunohistochemistry (IHC) of CYGB, were obtained from patients in Osaka City University Hospital (Osaka, Japan), who were diagnosed with NASH according to the classification of Matteoni et al.[17] Intact human specimens ($n = 3$) of nontumor lesions were obtained from patients who had metastasis liver tumors or cholangiocarcinoma treated by surgical resection. HCC tissues and noncancerous liver tissues were obtained from nine patients without hepatitis virus B or C infection, who had undergone a hepatectomy at the Osaka City University Hospital. They were patients with almost intact liver ($n = 2$), fatty liver ($n = 1$), liver fibrosis by undetermined etiology ($n = 1$), NASH ($n = 1$), and alcoholism ($n = 4$). The specimens were routinely processed, formalin fixed, and paraffin embedded. A portion of tissues was frozen and stored at −80°C without fixation. RNAs were extracted from them by the acid guanidinium thiocyanate-phenol-chloroform method, as described in our previous study.[18] All patients gave written informed consent to participate in this study in accordance with the ethical guidelines of the 1975 Declaration of Helsinki, and according to the process approved by the ethical committee of Osaka City University, Graduate School of Medicine.

Mice and Diet

C57BL/6 *Cygb* conventional knockout mice were generated in our laboratory, as described previously.[15] C57BL/6 mice (WT) were purchased from SLC (Shizuoka, Japan).

For the NASH model, 78 $Cygb^{-/-}$ and 77 WT mice were used, including males and females. Eight-week-old mice were fed CDAA (catalog 518753; Dyets, Bethlehem, PA) or a control diet, choline-supplied amino acid–defined diet (CSAA; catalog 518754; Dyets) with $n = 5$ to 14 per group. The CSAA control diet induces simple steatosis, but neither inflammation nor fibrosis, in WT mice[16] (Supplemental Figure S1). Mice were fed these diets continuously for 8, 16, or 32 weeks. To investigate tissue hypoxia, 1 hour before sacrifice, some mice were injected i.p. with hydroxyprobe-1 solution at a dose of 60 mg/kg body weight using the hydroxyprobe-1 Omni Kit (Hydroxyprobe, Burlington, MA), according to the manufacturer's protocol.

In the macrophage-depletion experiment, a subgroup of 20 mice were divided into four groups. A short 8-week protocol on the CDAA diet followed, with macrophage deletion in the final week, which was used to examine the early events of NASH. At the seventh week of CDAA feeding, Kupffer cell depletion was induced by injecting 200 μL liposomal clodronate (FormuMax Scientific, Palo Alto, CA) into the mouse tail vein, according to the manufacturer's protocol. Control mice were injected with the same amount of plain control liposomes. Mice were continuously fed the CDAA diet and sacrificed 1 week after injection.

For N-acetyl cysteine (NAC) treatment, a total of 53 $Cygb^{-/-}$ and WT mice, divided into six groups ($n = 5$ to 13 per group), were fed the CDAA diet, together with 0.1 mmol/L NAC (Sigma-Aldrich, St. Louis, MO) in the drinking water for 2, 8, or 32 weeks, starting at 8 weeks of age. NAC was prepared as a 0.5 mol/L stock in sterile water once a month, aliquoted, and stored at −30°C in the dark. Sterile drinking water was freshly made from the stock and changed twice a week. Animal care and procedures were approved by the Osaka City University Animal Care and Use Committee, as set forth in the NIH *Guide for the Care and Use of Laboratory Animals*.[19]

Histological, IHC, and Immunofluorescence Analysis

Hematoxylin and eosin, IHC, and immunofluorescence analyses were performed as previously described.[15] The primary antibodies used for mouse and human samples, including CYGB antibodies, were generated by our laboratory[6,15,20] and are described in Table 1. Pathological severity of nonalcoholic fatty liver disease was assessed using previously described criteria.[21] To quantify liver fibrosis, sections (5 μm thick) were stained with Picrosirius red (Sigma-Aldrich) and counterstained with Fast Green (Sigma-Aldrich). Collagen stained with Sirius Red was quantitated in the sections that were randomly chosen (<100 magnifications, 10 to 20 fields each from sample)

using Micro Analysis software version 1.1d (Thermo Scientific, West Palm Beach, FL). To quantify CYGB-positive cells in IHC staining, human liver normal ($n = 3$) and NASH sections ($n = 5$ in each group of NASH score ≤ 2, 3 to 6, and 7 to 8) were counted in at least 10 high-power fields (×400 magnification) per section.

DHE Assay

To examine the oxidative stress condition induced by CDAA diet and by the absence of CYGB, primary HSCs cultured as described below or freshly prepared frozen liver sections, which were warmed up at 37°C for 2 hours, were incubated with 2 μmol/L dihydroethidium (DHE; Invitrogen, Eugene, OR) in phosphate-buffered saline for 30 minutes at 37°C. Then, they were counterstained with DAPI and observed under fluorescent microscopy.

Hydroxyproline Assay

Hydroxyproline content of the liver was measured by a spectrophotometric assay by using Hydroxyproline Assay Kit (BioVision, Milpitas, CA), according to the assay protocol. Briefly, liver tissue was homogenized in ice-cold distilled water (100 μL of water for every 10 mg of tissue) using a polytron homogenizer. Subsequently, one volume of 12N HCl was added to the homogenized sample in a pressure-tight, Teflon-capped vial and was hydrolyzed for 3 hours at 120°C. After hydrolysis, 10 μL of each hydrolyzed sample was transferred to a 96-well plate and evaporated to dryness under vacuum. Then, samples were oxidized with chloramine-T (Sigma-Aldrich) for 5 minutes at room temperature. The reaction mixture was then incubated in dimethylaminobenzaldehyde at 60°C for 90 minutes and cooled to room temperature. A series of wells of hydroxyproline standard were prepared for each assay. Sample absorbance was measured at 560 nm. Hydroxyproline content was expressed as microgram of hydroxyproline per gram liver.

ALT Measurement

Alanine aminotransferase (ALT) activity (UV test at 37°C) was measured in serum using a commercially available kit (Wako, Osaka, Japan), according to manufacturer's protocol.

Quantitative Real-Time PCR

Total RNA was extracted from cells and liver tissues using the miRNeasy Mini Kit (Qiagen, Valencia, CA). cDNAs were synthesized using total RNA, a ReverTra Ace qPCR RT Kit (Toyobo, Osaka, Japan) and oligo(dT)$_{12\text{-}18}$ primers, according to the manufacturer's instructions. Gene expression was measured by real-time PCR using the cDNAs, SYBR qPCR Mix Reagents (Toyobo), and gene-specific oligonucleotide primers (Table 2) with an ABI Prism 7500 Fast Real-Time PCR System (Applied Biosystems, Foster, CA). Glyceraldehyde-3-phosphate dehydrogenase (Gapdh) level was used to normalize the relative abundance of mRNAs.

Gene Expression Profile for Specific Pathway

The Mouse Oxidative Stress and Antioxidant Defense RT^2 *Profiler* PCR Array from SA Biosciences (Frederick, MD; catalog PAMM-065) was performed to examine the expression of 84 genes related to oxidative stress, according

Table 1 Summary of Primary Antibodies Used for Immunohistochemistry or Immunofluorescences

Antigen*	Source	Name/clone; catalog no.	Incubation
AFP	US Biological (Swampscott, MA)	F4100-16A (Go)	O/N 4°C, 1:20
CD68	Abcam (Cambridge, UK)	Polyclonal (Rb); ab125212	O/N 4°C, 1:300
53PB1	Abcam	Polyclonal (Rb); ab36823	O/N 4°C, 1:300
CYGB	Our laboratory	Polyclonal (Rb) anti-mouse	O/N 4°C, 1:100
CYGB	Our laboratory	Monoclonal (Rb) anti-human	O/N 4°C, 1:100
p-AKT	Cell Signaling (Danvers, MA)	Monoclonal (Rb); 3787	O/N 4°C, 1:300
F4/80	eBioscience (San Diego, CA)	Monoclonal (Rt); 14-4801	O/N 4°C, 1:200
HO-1	Assay designs (Ann Arbor, MI)	Polyclonal (Rb); SPA-895	30 minutes room temperature, 1:100
Hydroxyprobe-1	Hydroxyprobe, Inc. (Burlington, MA)	Rb anti-pimonidazole; PAb2627	O/N 4°C, 1:100
iNOS	Abcam	Polyclonal (Rb); ab15203	O/N 4°C, 1:100
Ki-67	Abcam	Monoclonal (Rb); ab16667	O/N 4°C, 1:100
MPO	Abcam	Polyclonal (Rb); ab45977	O/N 4°C, 1:300
Neutrophil	Abcam	Monoclonal (Rt); ab2557	O/N 4°C, 1:100
Nitrotyrosine	Cell Signaling	Polyclonal (Rb); 9691	O/N 4°C, 1:100
p-ERK	Cell Signaling	Monoclonal (Rb); 4370	O/N 4°C, 1:200
αSma	Sigma-Aldrich	Monoclonal (Mo); clone: 1A4	O/N 4°C, 1:300
γH2AX	Novus Biologicals (Littleton, CO)	Monoclonal (Rb); NB100-79967	O/N 4°C, 1:200

*All antigens were retrieved by autoclaving for 15 minutes in 0.01 mol/L citrate buffer containing 0.05% Tween 20 (pH 6.0), except for Neutrophile and F4/80, in which proteinase K (400 μg/mL) in TE buffer (pH 8.0) was used.

AFP, α-fetoprotein; CYGB, cytoglobin; ERK, extracellular signal–regulated kinase; Go, goat; HO, heme oxygenase; H2AX, phosphorylated H2A histone protein, member X; iNOS, inducible nitric oxide synthase; Mo, mouse; MPO, myeloperoxidase; O/N, overnight; Rb, rabbit; Rt, rat; Sma, smooth muscle actin.

Table 2 Human and Mouse Primers Used for Quantitative Real-Time PCR

Primer name/ gene*	Sequence
*h*CYGB	F: 5′-TGCCAGTGACTTCCCACCT-3′
	R: 5′-TAGATGAGGCCACGCAGC-3′
*h*GAPDH	F: 5′-GCACCGTCAAGGCTGAGAAC-3′
	R: 5′-TGGTGAAGACGCCAGTGGA-3′
mAfp	F: 5′-CACACCCGCTTCCCTCAT-3′
	R: 5′-TTTTCGTGCAATGCTTTGGA-3′
mBcl2	F: 5′-AAGGGCTTCACACCCAAATCT-3′
	R: 5′-CTTCTACGTCTGCTTGGCTTTGA-3′
mCat	F: 5′-ATGGCTTTTGACCCAAGCAA-3′
	R: 5′-CGGCCCTGAAGCTTTTTGT-3′
mCcl3	F: 5′-TGAAACCAGCAGCCTTTGCTC-3′
	R: 5′-AGGCATTCAGTTCCAGGTCAGTG-3′
mCcl4	F: 5′-CCATGAAGCTCTGCGTGTCTG-3′
	R: 5′-GGCTTGGAGCAAAGACTGCTG-3′
mFos	F: 5′-CCCCAAACTTCGACCATGAT-3′
	R: 5′-GGAGGATGACGCCTCGTAGTC-3′
mJun	F: 5′-CCGCCCCTGTCCCCTAT-3′
	R: 5′-TCCTCATGCGCTTCCTCTCT-3′
mCol1a1	F: 5′-CCTCCCGCACCCAGTTC-3′
	R: 5′-CATCAGCATGTTTGGAGTAGTAAGC-3′
mCxcl1	F: 5′-TGAGCTGCGCTGTCAGTGCCT-3′
	R: 5′-AGAAGCCAGCGTTCACCAGA-3′
mCxcl2	F: 5′-GAGCTTGAGTGTGACGCCCCCAGG-3′
	R: 5′-GTTAGCCTTGCCTTTGTTCAGTATC-3′
mCxcl5	F: 5′-GCATTTCTGTTGCTGTTCACGCTG-3′
	R: 5′-CCTCCTTCTGGTTTTTCAGTTTAGC-3′
mCxcl7	F: 5′-TGGGCCTGATCCTTGTTGCGC-3′
	R: 5′-GCACCGTTTTTTGTCCATTCTTCAG-3′
mCcnd1	F: 5′-GCCCGGAGGGATTTGC-3′
	R: 5′-AGACGGAACACTAGAACCTAACAGATT-3′
mCygb	F: 5′-TGCATGACCCAGACAAGGTA-3′
	R: 5′-GGTCACGTGGCTGTAGATGA-3′
mGapdh	F: 5′-TGCACCACCAACTGCTTAG-3′
	R: 5′-GGATGCAGGGATGATGTTC-3′
mGpx6	F: 5′-GCCCAGAAGTTGTGGGGTTC-3′
	R: 5′-TCCATACTCATAGACGGTGCC-3′
mHo-1	F: 5′-GGTGATGGCTTCCTTGTACC-3′
	R: 5′-AGTGAGGCCCATACCAGAAG-3′
mHif1a	F: 5′-CAGTACAGGATGCTTGCCAAAA-3′
	R: 5′-ATACCACTTACAACATAATTCACACACACA-3′
mIl1b	F: 5′-CCATGGCACATTCTGTTCAAA-3′
	R: 5′-GCCCATCAGAGGCAAGGA-3′
mIl6	F: 5′-CCGCTATGAAGTTCCTCTCTGC-3′
	R: 5′-ATCCTCTGTGAAGTCTCCTCTCC-3′
m-iNos	F: 5′-CCTGGTACGGGCATTGCT-3′
	R: 5′-GCTCATGCGGCCTCCTTT-3′
mCcl2	F: 5′-GAGAGCCAGACGGGAGGAAG-3′
	R: 5′-TGAATGAGTAGCAGCAGGTGAG-3′
mMpo	F: 5′-CCATGGTCCAGATCATCACA-3′
	R: 5′-GCCGGTACTGATTGTTCAGG-3′
mTgfb1	F: 5′-GAGCCCGAAGCGGACTACT-3′
	R: 5′-TTGCGGTCCACCATTAGCA-3′
mTgfb3	F: 5′-AGGGCCCTGGACACCAATTAC-3′
	R: 5′-CCTTAGGTTCTGGGACCCATTTC-3′
mTimp1	F: 5′-ACTCGGACCTGGTCATAAGGGC-3′
	R: 5′-TTCCGTGGCAGGCAAGCAAAGT-3′
mTnfa	F: 5′-CTCTTCTCATTCCTGCTTGTGG-3′
	R: 5′-AATCGGCTGACGGTGTGG-3′
m-αSma	F: 5′-TCCCTGGAGAAGAGCTACGAACT-3′
	R: 5′-AAGCGTTCGTTTCCAATGGT-3′

*h, human; m, mouse.

CYGB, cytoglobin; F, forward; GAPDH, glyceraldehyde-3-phosphate dehydrogenase; iNos, inducible nitric oxide synthase; R, reverse; Sma, smooth muscle actin.

to manufacturer's protocol. Briefly, 1 μg of total RNA from 16-week-old CDAA-fed WT or $Cygb^{-/-}$ mice was used to make first-strand cDNA using RT^2 First Strand Kit (SA Biosciences). PCR mixture containing cDNA, distilled water, and SYBR Green master mix (SA Biosciences) was loaded into each well of 96-well plates containing the predispensed gene-specific primer sets, and PCR was performed with an ABI Prism 7500 Fast Real-Time PCR System (Applied Biosystems). The PCR was performed in 96-well plates with 84 genes related to oxidative stress, five housekeeping genes (*Actb*, *Gapdh*, *Hsp90ab1*, *Hprt1*, and *Gusb*) used for normalizing the PCR array data, one negative control to verify genomic DNA contamination, and three wells of RT controls to verify the efficiency of the RT reaction. The excel-based PCR array data analysis (SA Biosciences) was used to calculate the C_T values for all of the genes in the array. Then, fold changes in gene expression for pairwise comparison using the $\Delta\Delta C_T$ method were used to determine the relative expression levels of genes of interest for each sample.

Immunoblot Analysis

Protein samples (10 to 40 μg) were subjected to SDS-PAGE and transferred to Immobilon P membranes (Millipore Corp., Bedford, MA). After blocking, membranes were probed with primary antibodies against CYGB (1: 500) from our laboratory (Table 1), AKT (1:1000; Cell Signaling, Danvers, MA), phosphorylated AKT (1:500; Cell Signaling), BCL-2 (1:1000; Cell Signaling), extracellular signal–regulated kinase (ERK; 1:500; Cell Signaling), phosphorylated ERK (1:1000; Cell Signaling), CYCLIN D1 (1:5000; Cell Signaling), phosphorylated SMAD3 (1:1000; Abcam, Cambridge, UK), total SMAD3 (1:1000; Abcam), heme oxygenase-1 (HO-1; 1:1000; Cosmo Bio Co Ltd, Tokyo, Japan), myeloperoxidase (1:1000; Abcam), α-smooth muscle actin (α-Sma; 1:1000; Abcam), or GAPDH (1:2000; Santa Cruz Biotechnology, Santa Cruz, CA). Membranes were then incubated with horseradish peroxidase–conjugated secondary antibodies at 1:2000 dilutions. Immunoreactive bands

were visualized using the electrochemiluminescence detecting reagent (GE Healthcare UK Ltd, Buckinghamshire, UK), and documented with the Fujifilm Image Reader LAS-3000 (Fujifilm, Tokyo, Japan) coupled with image analysis software (Multi Gauge version 3.1; Fujifilm).

Cells

HSCs were isolated from WT ($HSC^{Cygb-wild}$) and $Cygb^{-/-}$ ($HSC^{Cygb-null}$) mice using the pronase-collagenase digestion method, as previously described,[22] and were cultured on uncoated plastic dishes (BD Falcon, Franklin Lake, NY) or glass chamber slides (Thermo Fisher Scientific, Waltham, MA) in Dulbecco's modified Eagle's medium (Sigma-Aldrich) supplemented with 10% fetal bovine serum (Invitrogen, Carlsbad, CA) and antibiotics (100 U/mL penicillin and 100 μg/mL streptomycin). $HSC^{Cygb-wild}$ and $HSC^{Cygb-null}$ cells were harvested at days 1, 4, and 7 for RNA, protein extractions, or for immunofluorescence, Oil Red O staining.

siRNA Transient Transfection

siRNA *Cygb* or the siRNA negative control (Ambion, Austin, TX) was transfected into $HSC^{Cygb-wild}$ using Lipofectamine RNAiMAX Transfection Reagent (Invitrogen, Carlsbad, CA) at a final concentration of 50 nmol/L, as previously described.[23] After 24 hours, the culture medium was changed to fresh Dulbecco's modified Eagle's medium (Sigma-Aldrich) supplemented with 10% fetal bovine serum (Invitrogen) and antibiotic. Then, after 72 hours, the cells were collected for total RNA extraction or after 96 hours, they were collected for protein extraction and for double immunofluorescence of α-SMA and HO-1.

Recombinant Human *CYGB* Treatment

Primary $HSC^{Cygb-null}$ mice were isolated from $Cygb^{-/-}$ mice and cultured on uncoated plastic dishes. After 24 hours, the culture medium was supplemented with 100 μg/mL of recombinant human *CYGB*.[10] And, after 72 hours, the cells were subjected for mRNA and protein analysis of α-SMA and CYGB expression.

Statistical Analysis

All data are expressed as the means ± SEM. Two groups were compared using an unpaired Student's *t*-test (two-tailed). $P < 0.05$ was considered statistically significant.

Results

Expression of CYGB in Human NASH and HCC

CYGB was originally identified in rat HSCs[6]; however, its expression in human NASH livers has remained undetermined. In normal human liver, CYGB was expressed in cells in Disse's space that contained lipid droplets and were negative for α-SMA, but not in hepatocytes (Figure 1A), indicating that CYGB-positive cells are HSCs. In NASH livers, the expression of CYGB declined in a negative correlation with increased NASH score (Figure 1B). A similar decline in CYGB protein (Figure 1C) and mRNA (Figure 1D) expression was observed in HCC regions. Therefore, a decline of CYGB expression likely contributes to the development of human NASH and liver cancer.

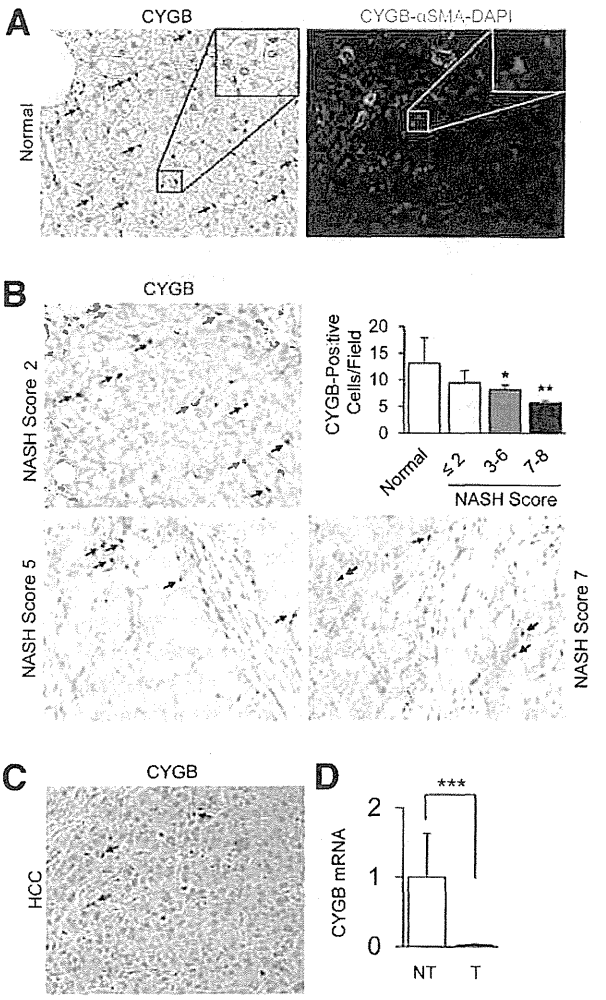

Figure 1 Expression of cytoglobin (CYGB) in human liver. **A:** Immunohistochemistry of CYGB and immunofluorescence of CYGB and α-smooth muscle actin (α-SMA) in normal human liver. **B:** Immunohistochemistry of CYGB and the quantification of its expression in human nonalcoholic steatohepatitis (NASH) livers with NASH score from 2 to 8. **C** and **D:** CYGB expression at the protein (**C**) and mRNA (**D**) levels in hepatocellular carcinoma [HCC; tumor (T)] and nontumor (NT) tissues derived from HCC patients without hepatitis B or C virus infection. **Arrows** indicate hepatic stellate cells. Data represent the means ± SD. $n = 3$ (**A**); $n = 5$ in each group (**B**); $n = 9$ (**C** and **D**). $^*P < 0.05$, $^{**}P < 0.01$, and $^{***}P < 0.001$. Original magnifications: ×400 (**A–C**); ×800 (**insets, A**).

Aggravation of Steatohepatitis and Liver Fibrosis in *Cygb* Deficiency

On the basis of observations in humans, we investigated Cygb involvement in the pathogenesis of NASH using $Cygb^{-/-}$ and WT mice fed a CDAA or control CSAA diet. The control diet induced simple steatosis in both sexes of WT mice, as shown by microscopy and hematoxylin and eosin staining (Supplemental Figure S1, A and B). WT mice fed the CDAA diet exhibited time-dependent hepatomegaly, as indicated by the increased liver per body weight ratio in both males and females. However, these ratios were significantly lower in $Cygb^{-/-}$ mice; those livers exhibited atrophy and surface irregularity, indicating liver fibrosis development (Supplemental Figure S1).

At as early as 8 weeks of CDAA treatment, the WT liver showed minor steatosis and almost no fibrosis development, whereas the $Cygb^{-/-}$ mouse liver exhibited inflammatory cell accumulation, including F4/80-positive macrophages, collagen deposition, especially along hepatic sinusoids, and prominent steatosis, as demonstrated by hematoxylin and eosin, Sirius Red, and Oil red O staining, respectively (Figure 2A). Concomitantly, the hepatocyte damage was more severe in $Cygb^{-/-}$ mice compared to WT mice, as indicated by the higher serum ALT level (Figure 2B). All of these changes were more obvious at 16 weeks and most severe at 32 weeks of CDAA feeding, as assessed by the Sirius Red–positive area, hydroxyproline content, and total NASH score (Figure 2, A–C). The absence of CYGB in HSCs (Supplemental Figure S2) induced markedly increased α-Sma expression, which clearly revealed the activation of HSCs from an early stage (Figure 2A), together with increased mRNA levels of α-Sma, collagen 1a1 (Figure 2D), tissue inhibitor of metalloproteinase 1, and transforming growth factor-β (data not shown) in the livers of $Cygb^{-/-}$ mice. Subsequently, phosphorylation of SMAD3, a key protein involved in the transforming growth factor-β–dependent fibrotic pathway, was up-regulated in $Cygb^{-/-}$ mice, indicative of the activation of a fibrotic signal in the early stage of CDAA diet feeding (Figure 2E). These results demonstrate that the absence of CYGB accelerates all aspects of the pathological processes of CDAA-induced steatohepatitis in mice.

Cygb Deficiency–Induced Inflammation and Liver Cancer Development

After 32 weeks of CDAA treatment, liver tumors developed in 100% of both male and female $Cygb^{-/-}$ mice, but never in their WT counterparts (Figure 2A and Supplemental Figure S1). The average number of nodules per mouse and the size of the nodules in male $Cygb^{-/-}$mice were 4.20 ± 3.39 mm and 3.81 ± 2.91 mm, respectively, which was smaller in female $Cygb^{-/-}$mice (Supplemental Figure S1). The liver tumor induction in female $Cygb^{-/-}$mice is surprising because WT female mice are usually resistant to tumor formation.[24,25]

The tumors in $Cygb^{-/-}$ livers had increased α-fetoprotein expression, Ki-67–positive nuclei, and ERK phosphorylation (Figure 3A). Expression of 53BP-1 and γH2AX, indicators of DNA double strain break, was markedly elevated in both tumor and nontumor regions of CDAA-fed $Cygb^{-/-}$ mouse livers, but were negligible in the WT mice (Figure 3A). Assuming that the DNA damage precedes the development of liver tumor, we assessed the γH2AX expression at earlier time points (8 or 16 weeks) on the CDAA and CSAA diet (Supplemental Figure S3A). γH2AX was negative in all CSAA groups, in both WT and $Cygb^{-/-}$ mice. In CDAA-treated mice, there were some γH2AX-positive hepatocytes in $Cygb^{-/-}$ mouse livers, but not in WT ones, at 8 or 16 weeks. In addition, mRNA expression for Afp, cytokines, such as Il-6, Il-1β, Tnf-α, and transforming growth factor-β1, and chemokines, such as Cxcl2 and Ccls 2 to 4, was significantly increased in $Cygb^{-/-}$ mice (Figure 3B). Their downstream targets, ERK, AKT, CYCLIN D1, and BCL-2, at the protein level, and cJun, cFos, Cyclin D1, and Bcl-2, at the mRNA level, were induced and activated in $Cygb^{-/-}$ mice fed a CDAA diet (Figure 3, C and D, and Supplemental Figure S3B). Therefore, *Cygb* deficiency triggers the early DNA damage and activation of ERK/AKT pathways, leading to the rapid progression of steatohepatitis to cancer development with CDAA treatment.

Increased Oxidative Stress in *Cygb* Deficiency

Next, because the CDAA diet induced oxidative stress[16] and Cygb can scavenger NO and ROS produced during oxidative stress,[10] we hypothesized that the oxidative stress conditions induced by a CDAA diet must be more stringent in the livers of $Cygb^{-/-}$ mice than in those of WT mice. Thus, we examined the level of ROS and related molecules in CDAA-treated $Cygb^{-/-}$ mice at the 32-week point. DHE staining showed stronger accumulation of red fluorescence in the nuclei of hepatocytes of $Cygb^{-/-}$ mice compared to WT mice (Figure 4A). Identical phenomenon was found from the 8-week point in CDAA-treated $Cygb^{-/-}$ mice, but not in WT ones and CSAA diet groups (Supplemental Figure S3C). In addition, we observed the following: i) an increase in hypoxic hepatocytes as shown by pimonidazole staining, ii) an induction of NO synthase and HO-1, and iii) high levels of nitrotyrosine formation in $Cygb^{-/-}$ mice (Figure 4, A and B). Taken together, these results indicate that the livers of CDAA-treated $Cygb^{-/-}$ mice were under stronger oxidative stress and hypoxia compared to corresponding WT mice.

Moreover, the oxidative stress and antioxidant defense PCR array revealed dysregulation of 31 genes, including an increase in pro-oxidant *Mpo* (39-fold) and a decrease in antioxidant genes after a 16-week CDAA treatment course (Table 3 and Supplemental Table S1). Increased *Mpo* and its main source, neutrophils, was confirmed (Figure 4C). These results are likely to correlate with the increased expression of inducible NO synthase, because myeloperoxidase is involved in $ONOO^-$ catabolism.[26] Therefore, the recruitment of

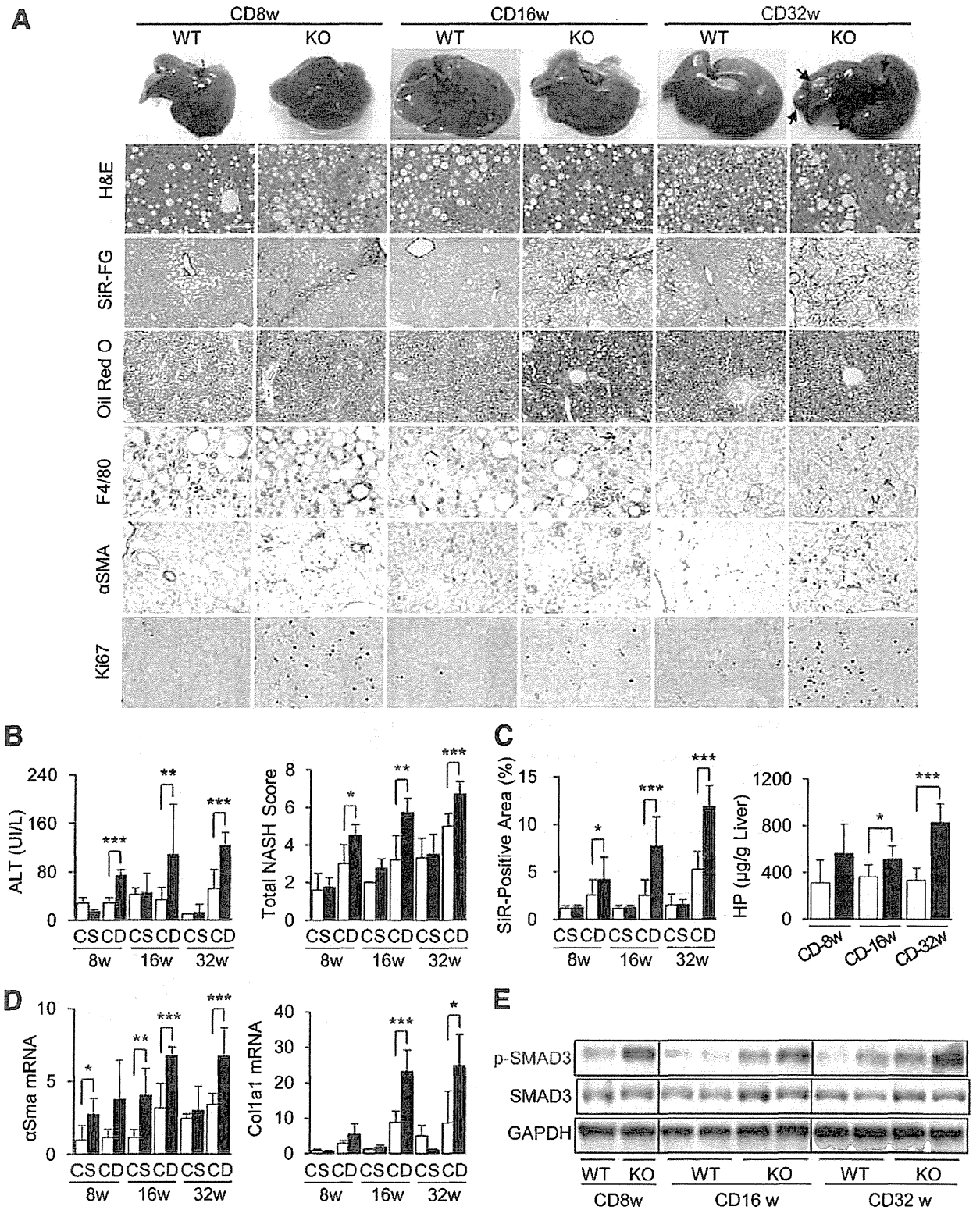

Figure 2 Promotion of hepatic steatosis and fibrosis in choline-deficient amino acid (CDAA)–fed *Cygb*$^{-/-}$ mice. Wild-type (WT) and *Cygb*$^{-/-}$ (KO) mice were fed choline-supplied amino acid (CS) or CDAA (CD) diets for 8, 16, or 32 weeks (w). **A:** Representative microscopic images and microscopic liver sections stained with hematoxylin and eosin (H&E), Sirius Red and Fast Green (SiR-FG), Oil Red O, and immunohistochemical staining for F4/80, α-smooth muscle actin (α-SMA), and Ki-67. The **arrows** indicate tumor nodules. **B:** Serum alanine aminotransferase (ALT) and total nonalcoholic steatohepatitis (NASH) score. **C:** Sirius Red–positive area and hydroxyproline (HP) content of the liver. **D:** Hepatic levels of α-Sma and collagen (Col) 1a1 mRNA. **E:** Immunoblots for phospho- and total SMAD3. Glyceraldehyde-3-phosphate dehydrogenase (GAPDH) is the loading control. White bar, WT; black bar, *Cygb*$^{-/-}$. Data represent the means ± SD. $n = 5$ to 14 per group. $^{*}P < 0.05$, $^{**}P < 0.01$, and $^{***}P < 0.001$. Original magnifications: ×200 (SiR-FG and Oil Red O; **A**); ×400 (H&E, F4/80, α-SMA, and Ki-67; **A**).

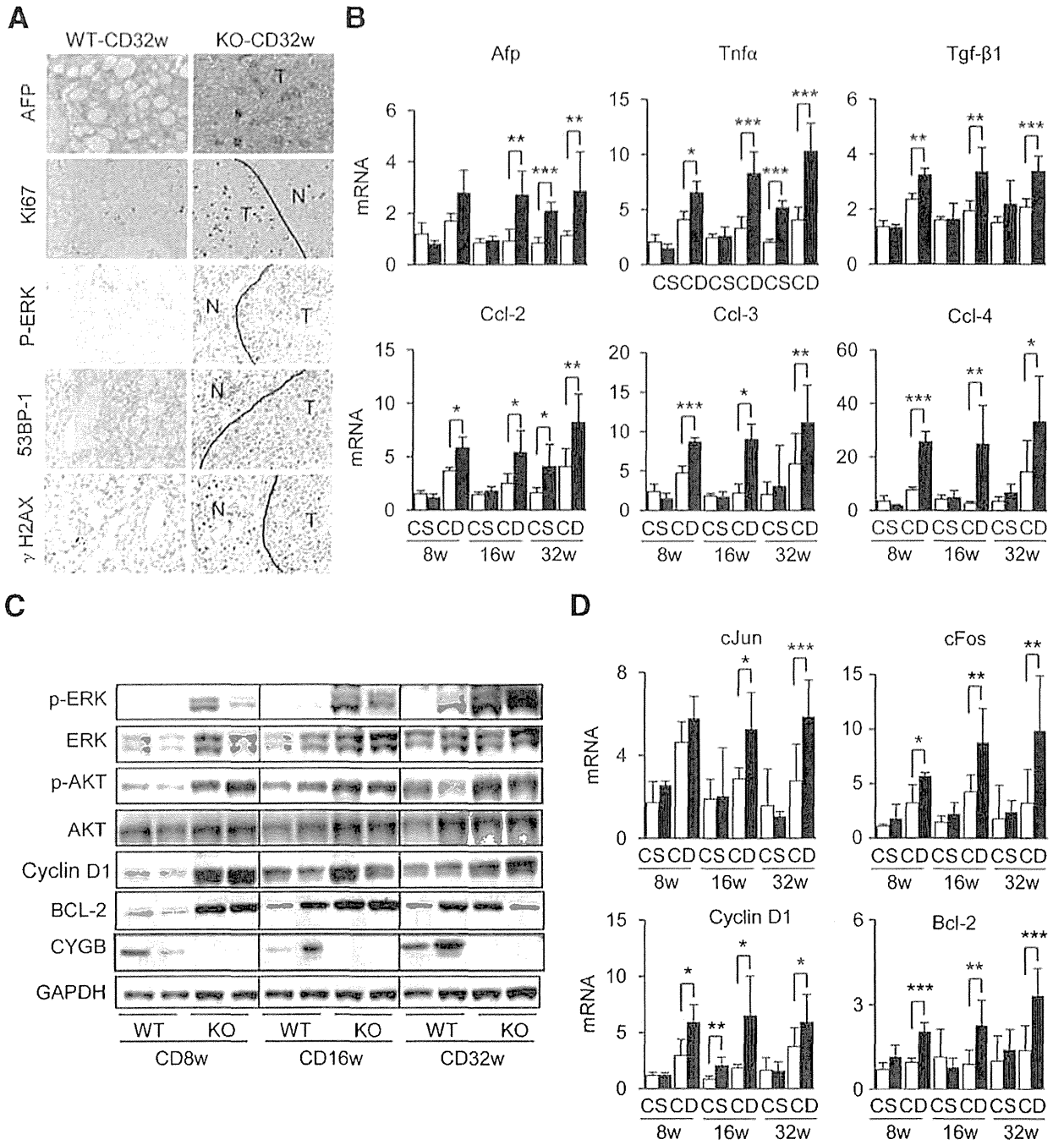

Figure 3 Augmentation of inflammation and liver cancer development in cytoglobin (CYGB) deficiency. **A:** Liver sections of 32-week choline-deficient amino acid (CDAA)—fed wild-type (WT) and *Cygb*$^{-/-}$ (KO) mice were immunostained for α-fetoprotein (AFP), Ki-67, p-extracellular signal–regulated kinase (ERK), 53PB-1, and phosphorylated H2A histone protein, member X (γH2AX). **B** and **C:** Nontumorous (N) liver tissues from WT (white bars) and *Cygb*$^{-/-}$ (black bars) mice from Figure 2 were examined for hepatic mRNA levels of Afp, cytokines, and chemokines (**B**) and immunoblotted for phospho- and total ERK and AKT, CYCLIN D1, BCL-2, and CYGB (**C**). Glyceraldehyde-3-phosphate dehydrogenase (GAPDH) is the loading control. **D:** Hepatic mRNA levels of cJun, cFos, Cyclin D1, and Bcl-2. Data represent the means ± SD. $*P < 0.05$, $**P < 0.01$, and $***P < 0.001$. Original magnification, ×400 (**A**). Ccl, chemokine ligand; T, tumor area; Tgf, transforming growth factor; Tnf, tumor necrosis factor.

neutrophils into the liver is suspected to participate in the augmentation of oxidative stress in the *Cygb*$^{-/-}$ mouse liver. In contrast, glutathione peroxidase 6 and catalase-1, enzymes that degrade H_2O_2, were down-regulated in *Cygb*$^{-/-}$ mice liver (Figure 4D) at the mRNA level.

Next, we examined whether HSCs themselves become imbalanced in terms of antioxidant/pro-oxidant levels in the absence of Cygb and generate excessive amounts of ROS and reactive nitrogen species in *Cygb*$^{-/-}$ mice. To test this, HSCs were isolated from the livers of WT and *Cygb*$^{-/-}$ mice

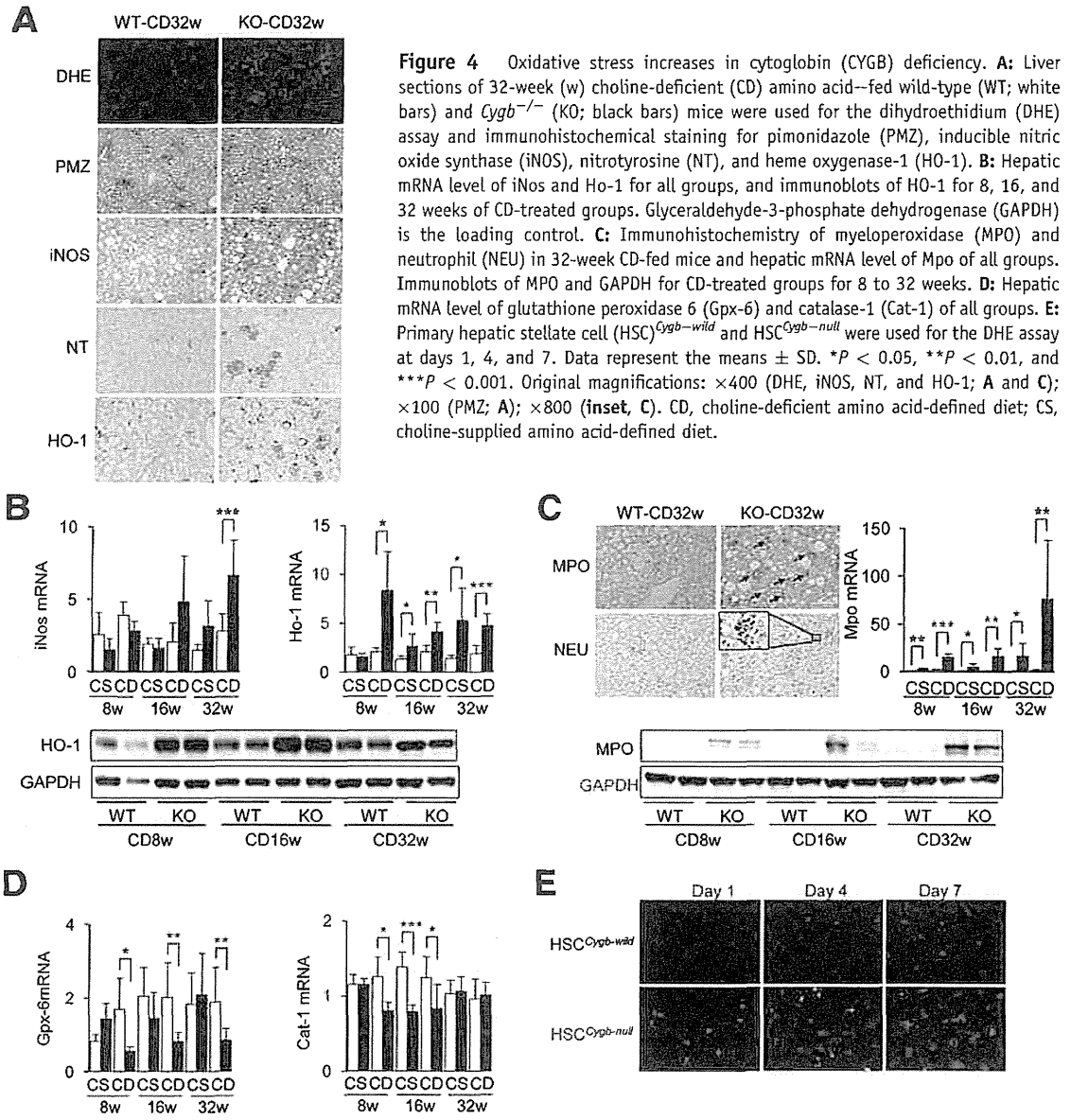

Figure 4 Oxidative stress increases in cytoglobin (CYGB) deficiency. **A:** Liver sections of 32-week (w) choline-deficient (CD) amino acid–fed wild-type (WT; white bars) and *Cygb*$^{-/-}$ (KO; black bars) mice were used for the dihydroethidium (DHE) assay and immunohistochemical staining for pimonidazole (PMZ), inducible nitric oxide synthase (iNOS), nitrotyrosine (NT), and heme oxygenase-1 (HO-1). **B:** Hepatic mRNA level of iNos and Ho-1 for all groups, and immunoblots of HO-1 for 8, 16, and 32 weeks of CD-treated groups. Glyceraldehyde-3-phosphate dehydrogenase (GAPDH) is the loading control. **C:** Immunohistochemistry of myeloperoxidase (MPO) and neutrophil (NEU) in 32-week CD-fed mice and hepatic mRNA level of Mpo of all groups. Immunoblots of MPO and GAPDH for CD-treated groups for 8 to 32 weeks. **D:** Hepatic mRNA level of glutathione peroxidase 6 (Gpx-6) and catalase-1 (Cat-1) of all groups. **E:** Primary hepatic stellate cell (HSC)$^{Cygb-wild}$ and HSC$^{Cygb-null}$ were used for the DHE assay at days 1, 4, and 7. Data represent the means ± SD. $^{*}P < 0.05$, $^{**}P < 0.01$, and $^{***}P < 0.001$. Original magnifications: ×400 (DHE, iNOS, NT, and HO-1; **A** and **C**); ×100 (PMZ; **A**); ×800 (**inset, C**). CD, choline-deficient amino acid-defined diet; CS, choline-supplied amino acid-defined diet.

(hereafter designated HSCs$^{Cygb-wild}$ and HSCs$^{Cygb-null}$, respectively) and stained for DHE (Figure 4E). It is clear that HSCs$^{Cygb-null}$ showed robust fluorescent products compared to HSCs$^{Cygb-wild}$ at any time point. Therefore, *Cygb* deficiency induced oxidative stress in HSCs in combination with the entire liver of mice fed the CDAA diet, resulting in irreversible liver injury.

Blunting Inflammation, Fibrosis, and Tumor Development Caused by Macrophage Depletion and N-Acetyl Cysteine Administration in *Cygb*$^{-/-}$ Mice

It is already known that activated HSCs attract and stimulate macrophages with multiple chemokines and macrophage colony-stimulating factor, and macrophages produce profibrotic mediators that directly activate fibroblasts.[27] To gain insight into the counteraction between activated HSCs and macrophages at the onset of steatohepatitis, mice fed CDAA for 8 weeks were subjected to macrophage depletion (Supplemental Figure S4). As a result, all of the features of NASH were attenuated significantly in WT and *Cygb*$^{-/-}$ mice (Figure 5, A and D); decreased hepatic mRNA expression levels of cytokines and fibrogenic genes (Figure 5, B and C) and of phospho- and total ERK and HO-1 at the protein level were evident (Figure 5E). Taken together, these data suggest that the macrophages, in addition to the activated HSCs, contributed to the magnification of fibroinflammatory reaction from the early stage of steatohepatitis in *Cygb*$^{-/-}$ mice.

Next, we assessed whether NAC, a well-known anti-oxidative agent, is able to ameliorate the oxidative

Table 3 List of Oxidative Defense and Antioxidant Genes Induced or Inhibited in $Cygb^{-/-}$ Mice Fed CDAA Diet for 16 Weeks Compared with WT

Classification	Group	Symbol	Fold regulation	*P* value
Antioxidants	GPx	*Gpx2*	5.4179	0.004459
		Gpx3	3.9264	0.005983
		Gpx8	2.43	0.022254
		Gpx6	−2.0372	0.045704
		Gstk1	−2.1017	0.008496
		Cat	−2.2167	0.038964
		Apc	−1.2518	0.017928
		Gpx1	−1.6357	0.001067
	TPx	*Ehd2*	2.2165	0.011267
	Other peroxidases	*Mpo*	39.1506	0.02483
		Ptgs2	4.3157	0.007775
		Aass	−2.1207	0.008114
		Serpinb1	−3.274	0.047218
		Prdx6-ps1	−1.7729	0.009071
	Other antioxidants	*Nxn*	2.1284	0.00469
		Srxn1	2.4743	0.015928
		Txnrd3	−1.2862	0.01688
Genes involved in ROS metabolism	SODs	*Sod1*	−1.7411	0.008437
		Sod2	−1.8508	0.003687
	Superoxide metabolism	*Cyba*	2.4659	0.005922
		Ncf2	1.8944	0.043651
		Ccs	−1.8331	0.018322
	Oxidative stress response genes	*Ucp3*	3.1634	0.048224
		Park7	−1.2894	0.011379
		Apoe	−1.3402	0.027972
		Idh1	−1.4476	0.036943
		Prdx1	−1.4531	0.010922
		Prdx6	−2.0804	0.005798
		Psmb5	−1.2492	0.009211
		Xpa	−1.4258	0.021297
Oxygen transporters		*Cygb*	−5.2371	0.000173
		Vim	2.6015	0.07583

The significance of the change in gene expression between the two groups was evaluated by unpaired Student's *t*-test for each gene. The level of statistical significance is set at $P < 0.05$. $n = 3$ for each group.

CDAA, choline-deficient amino acid; GPx, glutathione peroxidases; ROS, reactive oxygen species; SOD, superoxide dismutase; TPx, peroxiredoxins; WT, wild type.

stress–induced activation of HSCs and liver tumor formation in $Cygb^{-/-}$ mice. After CDAA feeding for 8, but not 2, weeks, $Cygb^{-/-}$ mice cotreated with 0.1 mmol/L NAC in drinking water had gained liver weight and reduced fibrosis level, as those of CDAA-treated WT mice (Supplemental Figure S5, A and B). NAC treatment also blunted the increase in $CD68^+$ cells (Supplemental Figure S5A) and attenuated the expression of all of the markers examined (ie, iNos, Ho-1, Tnf-α, and α-Sma) in CDAA-treated $Cygb^{-/-}$ mice (Supplemental Figure S5, B and C).

These phenomena were found with prolonged NAC treatment for 32 weeks, with impressively reduced liver tumor formation (in terms of frequency, numbers, and sizes) compared to the non-NAC group (Figure 6, A and B). The down-regulation of oxidative stress markers (Figure 6C) subsequently induced decreases in α-SMA, an HSC activation marker, and the Sirius Red–positive area (Figure 6, A, D, and E), $CD68^+$ cells, and inflammatory cytokines and chemokines (Figure 6, A and F); and proliferating hepatocytes, as shown by Ki-67 staining (Figure 6A). Overall, blunting oxidative stress mostly reduced HSC activation, fibrosis development, and ultimately tumor formation in CDAA-treated $Cygb^{-/-}$ mice.

Cygb Deficiency Triggers HSC Priming

All of the above results indicate that the severe fibrosis and cancer development in CDAA-fed $Cygb^{-/-}$ mice is related to HSC activation. We speculated that primary HSCs from $Cygb^{-/-}$ mice possess a characteristic preactivated phenotype or priming condition that is rapidly fully activated on a CDAA diet. To test this hypothesis, purified HSCs from WT and $Cygb^{-/-}$ mice were subjected to phenotype analyses. Cytologically, $HSCs^{Cygb-null}$ lost cellular lipid droplets more rapidly than $HSCs^{Cygb-wild}$, and became enlarged with a developed α-SMA network after 7 days in culture (Figure 7A). Interestingly, we found marked increases in the mRNA expression of fibrogenesis-related genes (αSma,

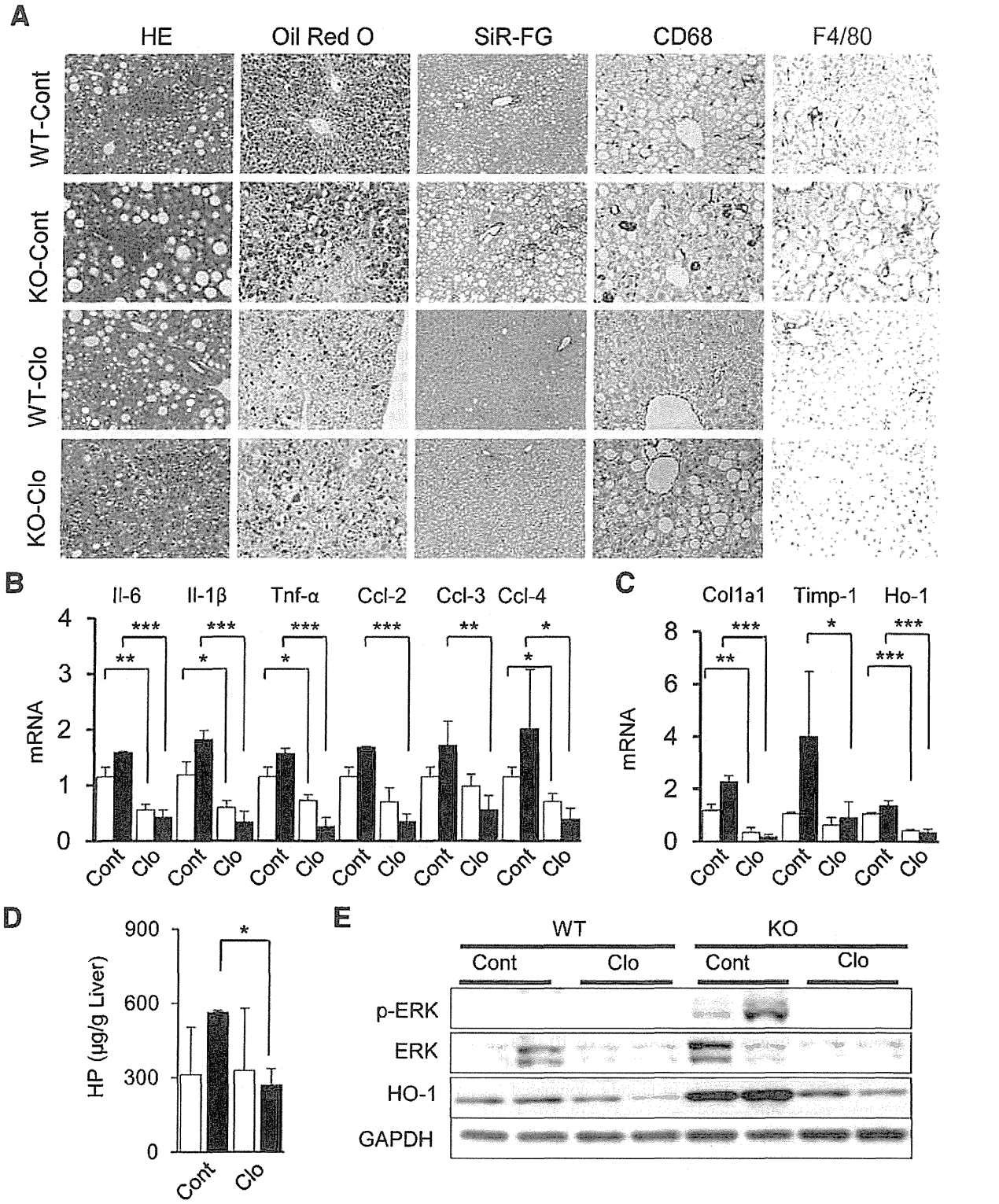

Figure 5 Effect of macrophage depletion in inflammation and fibrosis in *Cygb*$^{-/-}$ mice. Wild-type (WT; white bars) and *Cygb*$^{-/-}$ (KO; black bars) mice were injected with liposomal clodronate (Clo) or plain control liposomes (Cont) at 7 weeks in mice fed the choline-deficient amino acid (CDAA) diet for a total of 8 weeks. **A:** Liver sections were stained with hematoxylin and eosin (H&E), Oil Red O, Sirius Red and Fast Green (SiR-FG), and immunohistochemical staining for CD68 and F4/80. **B** and **C:** Hepatic mRNA level of cytokines, chemokines (**B**), and fibrogenesis-related genes (**C**). **D:** Hydroxyproline (HP) content of the liver. **E:** Immunoblots of phospho- and total extracellular signal–regulated kinase (ERK) and heme oxygenase-1 (HO-1). Glyceraldehyde-3-phosphate dehydrogenase (GAPDH) is the loading control. Data represent the means ± SD. $n = 5$ per group. $^{*}P < 0.05$, $^{**}P < 0.01$, and $^{***}P < 0.001$. Original magnifications: ×200 (SiR-FG and Oil Red O; **A**); ×400 (H&E, F4/80, and CD68; **A**). Ccl, chemokine ligand; Col, collagen; Timp, tissue inhibitor of metalloproteinase; Tnf, tumor necrosis factor.

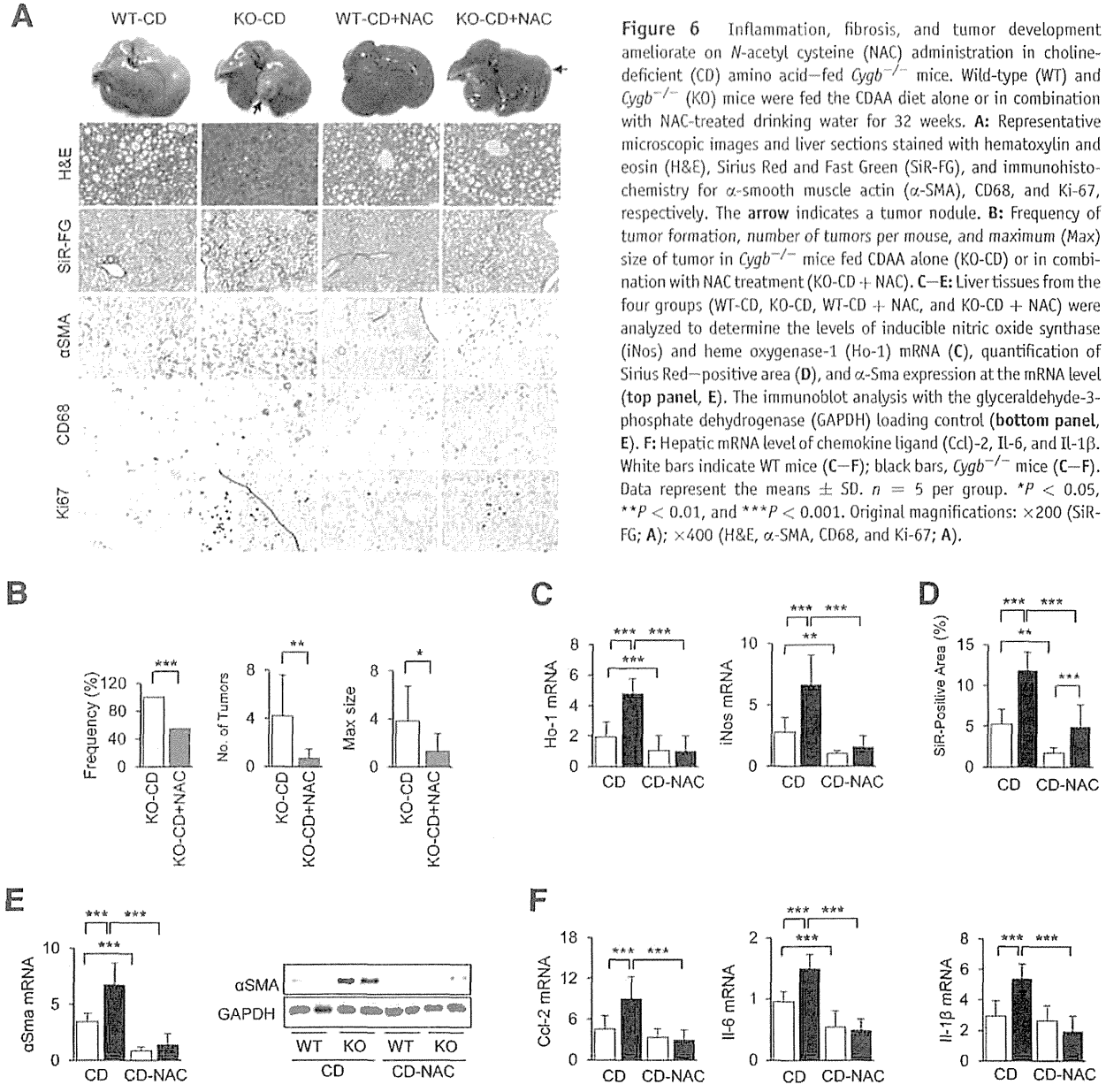

Figure 6 Inflammation, fibrosis, and tumor development ameliorate on *N*-acetyl cysteine (NAC) administration in choline-deficient (CD) amino acid–fed *Cygb*$^{-/-}$ mice. Wild-type (WT) and *Cygb*$^{-/-}$ (KO) mice were fed the CDAA diet alone or in combination with NAC-treated drinking water for 32 weeks. **A:** Representative microscopic images and liver sections stained with hematoxylin and eosin (H&E), Sirius Red and Fast Green (SiR-FG), and immunohistochemistry for α-smooth muscle actin (α-SMA), CD68, and Ki-67, respectively. The **arrow** indicates a tumor nodule. **B:** Frequency of tumor formation, number of tumors per mouse, and maximum (Max) size of tumor in *Cygb*$^{-/-}$ mice fed CDAA alone (KO-CD) or in combination with NAC treatment (KO-CD + NAC). **C–E:** Liver tissues from the four groups (WT-CD, KO-CD, WT-CD + NAC, and KO-CD + NAC) were analyzed to determine the levels of inducible nitric oxide synthase (iNos) and heme oxygenase-1 (Ho-1) mRNA (**C**), quantification of Sirius Red–positive area (**D**), and α-Sma expression at the mRNA level (**top panel, E**). The immunoblot analysis with the glyceraldehyde-3-phosphate dehydrogenase (GAPDH) loading control (**bottom panel, E**). **F:** Hepatic mRNA level of chemokine ligand (Ccl)-2, Il-6, and Il-1β. White bars indicate WT mice (**C–F**); black bars, *Cygb*$^{-/-}$ mice (**C–F**). Data represent the means ± SD. $n = 5$ per group. $^{*}P < 0.05$, $^{**}P < 0.01$, and $^{***}P < 0.001$. Original magnifications: ×200 (SiR-FG; **A**); ×400 (H&E, α-SMA, CD68, and Ki-67; **A**).

Col1α1, and Timp-1), cytokines (Il-6, Tnf-α, and Il-1β), and chemokines (Cxcls 1, 2, 5, and 7 and Ccls 2, 3, and 4) (Figure 7B) in HSCs$^{Cygb-null}$ at 1 day in culture, compared with HSC$^{Cygb-wild}$. These differences remained until day 4, but were lost by day 7 (data not shown). Immunoblot showed an increased expression of HO-1 and p-ERK in HSCs$^{Cygb-null}$ at 1 day (Figure 7C). Similar to HSCs$^{Cygb-null}$, HSCs$^{Cygb-wild}$ transfected with *Cygb* siRNA became morphologically enlarged and expressed more mRNAs and proteins than the negative control (Figure 7, D and E). In contrast, HSCs$^{Cygb-null}$ treated with 100 μg/mL of recombinant human CYGB for 72 hours showed marked reduction in α-SMA mRNA and protein expression and maintained their quiescent morphological features (Figure 7F). Taken together, the loss of *Cygb* both *in vitro* and *in vivo* induced priming conditions in which the cells expressed high levels of fibroinflammatory genes and produced ROS.

Discussion

The current study showed that the key pathological characteristics of NASH, including fatty degeneration of hepatocytes accompanied by ROS formation, inflammation, and fibrosis, were markedly accelerated in a time-dependent manner in CDAA-fed *Cygb*$^{-/-}$ mice. In addition, the unexpected development of HCC in all of the *Cygb*$^{-/-}$ mice is noteworthy.

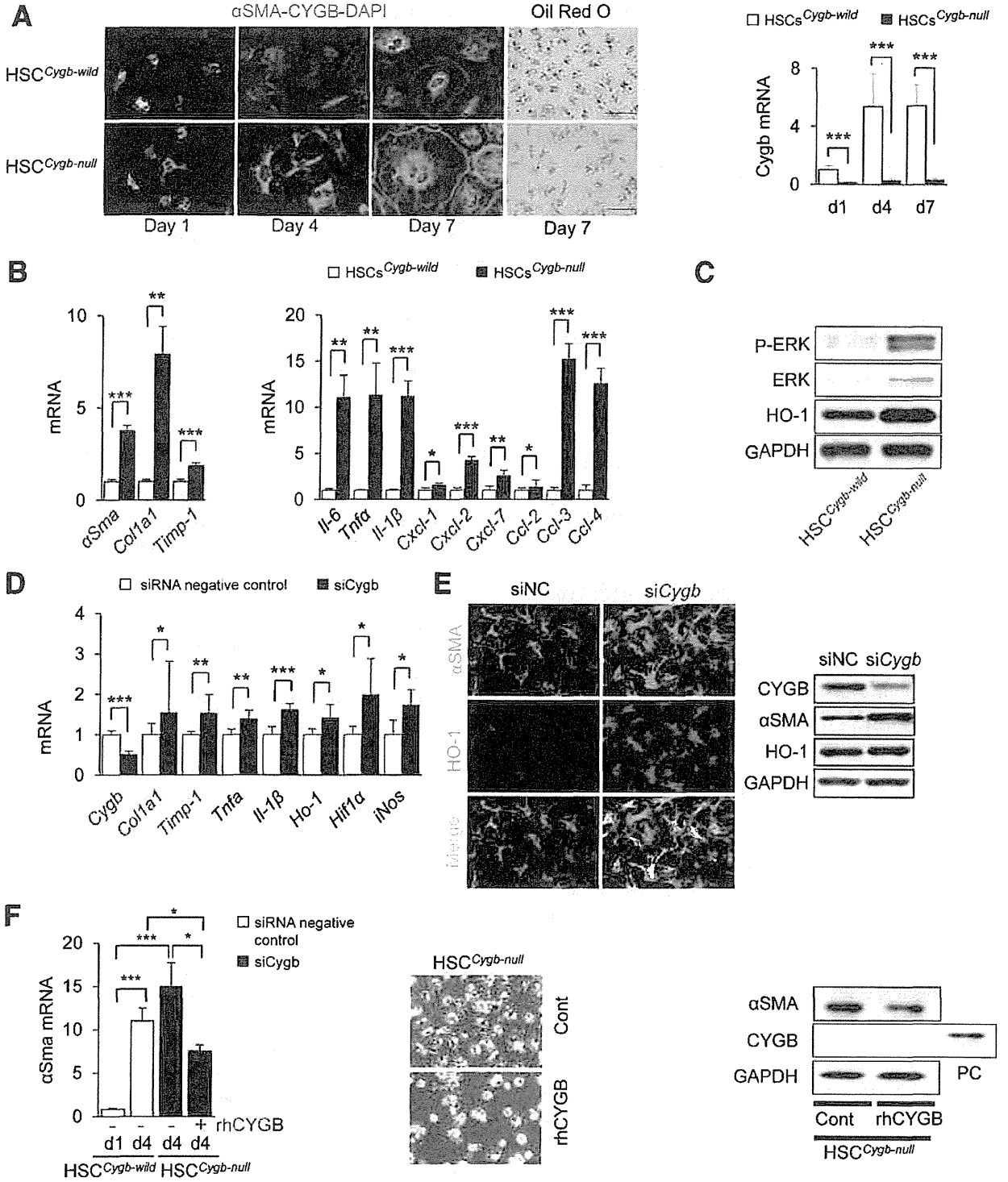

Figure 7 Priming hepatic stellate cells (HSCs) under cytoglobin (Cygb) deficiency. Primary mouse HSCs$^{Cygb-wild}$ and HSCs$^{Cygb-null}$ were cultured for days (d) 1, 4, and 7. **A:** Representative confocal images of α-smooth muscle actin (α-SMA; green) and CYGB (red) double stain. Oil Red O staining was performed, and *Cygb* expression at the mRNA level was determined. **B:** mRNA expression of genes for fibrogenesis, cytokines, and chemokines at day 1. **C:** Immunoblots of phospho- and total extracellular signal–regulated kinase (ERK) and heme oxygenase-1 (HO-1) at day 1. Glyceraldehyde-3-phosphate dehydrogenase (GAPDH) is the loading control. **D** and **E:** Primary mouse HSCs$^{Cygb-wild}$ were isolated and transiently transfected with siRNA *Cygb* (si*Cygb*) or siRNA-negative control for 24 hours. **D:** mRNA expression of fibrogenesis and oxidative stress markers. **E:** Representative confocal images of double staining of α-SMA (green) and HO-1 (red). Immunoblots of CYGB, α-SMA, HO-1, and GAPDH. **F:** Primary mouse HSCs$^{Cygb-null}$ were isolated and treated with human recombinant CYGB (rhCYGB) at the concentration of 100 μg/mL or fresh medium (Cont) for 72 hours of α-Sma expression at the mRNA and protein level and cell morphological features. Data represent the means ± SD. $n = 4$ to 6 per group. $^*P < 0.05$, $^{**}P < 0.01$, and $^{***}P < 0.001$. Original magnification, ×400 (**E**). Ccl, chemokine ligand; Col, collagen; iNos, inducible nitric oxide synthase; PC, rhCYGB serves as a positive control; Timp, tissue inhibitor of metalloproteinase; Tnf, tumor necrosis factor.

Augmented Inflammatory Cell Infiltration with *Cygb* Deficiency

Increased ALT levels in $Cygb^{-/-}$ mice indicated more severe hepatocyte damage than that of WT mice with CDAA feeding. In addition, we found an increased number of ballooning hepatocytes that contained Mallory bodies in $Cygb^{-/-}$ mice (Figure 2B). The ballooned hepatocytes probably reflect imminent cell necrosis, which leads to the activation of macrophages, neutrophils, and other proinflammatory pathways.[28]

Infiltration of the CDAA-fed $Cygb^{-/-}$ mouse liver by macrophages and neutrophils was extremely pronounced from 8 weeks onward, and was accompanied by augmented cytokine and chemokine expression (Figure 3B). *Ccl-2* is believed to activate HSCs and immune cells while exacerbating hepatic inflammation and cell death, contributing to the development of NASH fibrosis.[29] *Ccl-3* and *Ccl-4* trigger the recruitment of monocyte-derived macrophages and neutrophils in the liver with NASH.[5,30] Thus, augmented chemokine production in *Cygb* deficiency promotes inflammatory cell infiltration.

Aggravation of Oxidative Stress Conditions with *Cygb* Deficiency

CYGB was down-regulated with human NASH and HCC, whereas the absence of *Cygb* promotes NASH and HCC development in CDAA-treated mice. This suggests the requirement of CYGB for homeostasis in the human liver. Previous reports indicated the protective role that *Cygb* plays in protection against oxidative stress in human neuronal cell lines[31–33] and in rat HSCs.[34] Our results revealed that, in addition to up-regulated pro-oxidative genes and down-regulated antioxidative genes, reactive nitrogen species accumulated in the $Cygb^{-/-}$ mouse liver treated with the CDAA diet. This implies the role of *Cygb* in O_2-dependent NO removal as NO dioxygenase.[35] Taken together, *Cygb* plays a pivotal role in the control of ROS and reactive nitrogen species in the inflamed liver.

Role of Cygb in the NASH Fibrotic Reaction

HSCs play an important role in remodeling the extracellular matrix and the progression of fibrosis in NASH.[12] Reactive oxygen intermediates, apoptotic bodies from hepatocytes, and paracrine stimuli from Kupffer cells trigger HSC activation.[36] We found that loss of *Cygb* also induced the priming of HSCs, which amplified the expression of fibrogenesis-related genes, cytokines, and a variety of chemokines (Figure 7). The priming of HSCs probably contributes to the immediate progression of fibrosis in $Cygb^{-/-}$ mice. In contrast, *Cygb* transgenic rats exhibited slow progression of fibrosis with an ischemia-reperfusion kidney injury.[37] Therefore, the antifibrotic function of CYGB could be illuminative.

With regard to CYGB expression and HSC activation, we reported stellate cell activation–associated protein (original name of CYGB) and its increased expression in rat HSCs during primary culture, and in those isolated from fibrotic rat livers compared to those from normal rat livers.[6] Herein, we additionally found the up-regulation of CYGB on primary-cultured mouse wild-type HSCs *in vitro* until day 7 and absence of CYGB in knockouts augmented HSC activation (Figure 7). In patients with NASH, the more fibrosis developed, the less CYGB expressed in HSCs (Figure 1B). Taken together, these phenomena indicate that CYGB may be transiently induced at the early stage of HSC activation and decelerate their activation process, although the exact role of CYGB in the early stage of HSC activation should be studied further.

Role of Cygb in Cancer Development with NASH

The role of *Cygb* as a tumor-suppressor gene has been reported in several human cancerous tissues and cancer cell lines. McRonald et al[12] first reported that CYGB expression was down-regulated in tylotic esophageal biopsy specimens. Several reports have examined the decreased expression of CYGB and the hypermethylation of the *CYGB* promoter in non-small cell lung carcinoma tissues and head and neck cancer, among others.[11–14,38] Shivapurkar et al[39] reported the augmented growth of NCI-H661 lung cancer cells with siCYGB treatment, and the suppression of NCI-H228 cell proliferation when transfected with CYGB cDNA. We previously reported that *Cygb*-null mice showed susceptibility to liver tumor development under diethylnitrosamine treatment.[15] These reports, along with our present study, indicate the tumor-suppressor role of *Cygb*.

DNA and aberrant mutations are known to accumulate in chronically damaged liver tissue.[40] γH2AX, an indicator of a DNA double-stranded break, was increased in many human cancers,[41] human preneoplastic HCC lesions,[42] and inflamed cancer tissues.[43] Herein, we observed the expression of γH2AX and 53BP-1 in nontumor tissue regions and in tumors in *Cygb*-null mice (Figure 3A and Supplemental Figure S3A). Furthermore, oncogenic ERK and AKT, which are constitutively phosphorylated with HCC,[40] were activated early in our model (Figure 3C).

In summary, *Cygb* plays an important role in liver fibrosis and carcinogenesis through the control of HSC activation and ROS formation with a CDAA diet. The antitumorigenic and antifibrosis activity of *Cygb* is not only model specific but may also apply to human NASH and liver cancer development.

Acknowledgments

We thank Drs. Kazuo Ikeda and Masaru Enomoto for helpful discourse and Hirano Yukiko for technical assistance.

Supplemental Data

Supplemental material for this article can be found at *http://dx.doi.org/10.1016/j.ajpath.2014.12.017.*

References

1. Pessayre D, Berson A, Fromenty B, Mansouri A: Mitochondria in steatohepatitis. Semin Liver Dis 2001, 21:57–69
2. Day CP, James OF: Steatohepatitis: a tale of two "hits"? Gastroenterology 1998, 114:842–845
3. Starley BQ, Calcagno CJ, Harrison SA: Nonalcoholic fatty liver disease and hepatocellular carcinoma: a weighty connection. Hepatology 2010, 51:1820–1832
4. Ramadori G, Armbrust T: Cytokines in the liver. Eur J Gastroenterol Hepatol 2001, 13:777–784
5. Schwabe RF, Seki E, Brenner DA: Toll-like receptor signaling in the liver. Gastroenterology 2006, 130:1886–1900
6. Kawada N, Kristensen DB, Asahina K, Nakatani K, Minamiyama Y, Seki S, Yoshizato K: Characterization of a stellate cell activation-associated protein (STAP) with peroxidase activity found in rat hepatic stellate cells. J Biol Chem 2001, 276:25318–25323
7. Burmester T, Ebner B, Weich B, Hankeln T: Cytoglobin: a novel globin type ubiquitously expressed in vertebrate tissues. Mol Biol Evol 2002, 19:416–421
8. Sawai H, Kawada N, Yoshizato K, Nakajima H, Aono S, Shiro Y: Characterization of the heme environmental structure of cytoglobin, a fourth globin in humans. Biochemistry 2003, 42:5133–5142
9. Nakatani K, Okuyama H, Shimahara Y, Saeki S, Kim DH, Nakajima Y, Seki S, Kawada N, Yoshizato K: Cytoglobin/STAP, its unique localization in splanchnic fibroblast-like cells and function in organ fibrogenesis. Lab Invest 2004, 84:91–101
10. Sugimoto H, Makino M, Sawai H, Kawada N, Yoshizato K, Shiro Y: Structural basis of human cytoglobin for ligand binding. J Mol Biol 2004, 339:873–885
11. Xinarianos G, McRonald FE, Risk JM, Bowers NL, Nikolaidis G, Field JK, Liloglou T: Frequent genetic and epigenetic abnormalities contribute to the deregulation of cytoglobin in non-small cell lung cancer. Hum Mol Genet 2006, 15:2038–2044
12. McRonald FE, Liloglou T, Xinarianos G, Hill L, Rowbottom L, Langan JE, Ellis A, Shaw JM, Field JK, Risk JM: Down-regulation of the cytoglobin gene, located on 17q25, in tylosis with oesophageal cancer (TOC): evidence for trans-allele repression. Hum Mol Genet 2006, 15:1271–1277
13. Presneau N, Dewar K, Forgetta V, Provencher D, Mes-Masson AM, Tonin PN: Loss of heterozygosity and transcriptome analyses of a 1.2 Mb candidate ovarian cancer tumor suppressor locus region at 17q25.1-q25.2. Mol Carcinog 2005, 43:141–154
14. Shaw RJ, Omar MM, Rokadiya S, Kogera FA, Lowe D, Hall GL, Woolgar JA, Homer J, Liloglou T, Field JK, Risk JM: Cytoglobin is upregulated by tumour hypoxia and silenced by promoter hypermethylation in head and neck cancer. Br J Cancer 2009, 101:139–144
15. Thuy le TT, Morita T, Yoshida K, Wakasa K, Iizuka M, Ogawa T, Mori M, Sekiya Y, Momen S, Motoyama H, Ikeda K, Yoshizato K, Kawada N: Promotion of liver and lung tumorigenesis in DEN-treated cytoglobin-deficient mice. Am J Pathol 2011, 179:1050–1060
16. Denda A, Kitayama W, Kishida H, Murata N, Tsutsumi M, Tsujiuchi T, Nakae D, Konishi Y: Development of hepatocellular adenomas and carcinomas associated with fibrosis in C57BL/6J male mice given a choline-deficient, L-amino acid-defined diet. Jpn J Cancer Res 2002, 93:125–132
17. Matteoni CA, Younossi ZM, Gramlich T, Boparai N, Liu YC, McCullough AJ: Nonalcoholic fatty liver disease: a spectrum of clinical and pathological severity. Gastroenterology 1999, 116:1413–1419
18. Tamori A, Nishiguchi S, Kubo S, Koh N, Moriyama Y, Fujimoto S, Takeda T, Shiomi S, Hirohashi K, Kinoshita H, Otani S, Kuroki T: Possible contribution to hepatocarcinogenesis of X transcript of hepatitis B virus in Japanese patients with hepatitis C virus. Hepatology 1999, 29:1429–1434
19. Committee for the Update of the Guide for the Care and Use of Laboratory Animals; National Research Council: Guide for the Care and Use of Laboratory Animals. Eighth Edition. Washington, DC, National Academies Press, 2011
20. Motoyama H, Komiya T, Thuy le TT, Tamori A, Enomoto M, Morikawa H, Iwai S, Uchida-Kobayashi S, Fujii H, Hagihara A, Kawamura E, Murakami Y, Yoshizato K, Kawada N: Cytoglobin is expressed in hepatic stellate cells, but not in myofibroblasts, in normal and fibrotic human liver. Lab Invest 2014, 94:192–207
21. Kleiner DE, Brunt EM, Van Natta M, Behling C, Contos MJ, Cummings OW, Ferrell LD, Liu YC, Torbenson MS, Unalp-Arida A, Yeh M, McCullough AJ, Sanyal AJ: Design and validation of a histological scoring system for nonalcoholic fatty liver disease. Hepatology 2005, 41:1313–1321
22. Bach Kristensen D, Kawada N, Imamura K, Miyamoto Y, Tateno C, Seki S, Kuroki T, Yoshizato K: Proteome analysis of rat hepatic stellate cells. Hepatology 2000, 32:268–277
23. Sekiya Y, Ogawa T, Iizuka M, Yoshizato K, Ikeda K, Kawada N: Down-regulation of cyclin E1 expression by microRNA-195 accounts for interferon-beta-induced inhibition of hepatic stellate cell proliferation. J Cell Physiol 2011, 226:2535–2542
24. Vesselinovitch SD: The sex-dependent difference in the development of liver tumors in mice administered dimethylnitrosamine. Cancer Res 1969, 29:1024–1027
25. Naugler WE, Sakurai T, Kim S, Maeda S, Kim K, Elsharkawy AM, Karin M: Gender disparity in liver cancer due to sex differences in MyD88-dependent IL-6 production. Science 2007, 317:121–124
26. Shao B, Oda MN, Oram JF, Heinecke JW: Myeloperoxidase: an oxidative pathway for generating dysfunctional high-density lipoprotein. Chem Res Toxicol 2010, 23:447–454
27. Wynn TA, Barron L: Macrophages: master regulators of inflammation and fibrosis. Semin Liver Dis 2010, 30:245–257
28. Kono H, Rock KL: How dying cells alert the immune system to danger. Nat Rev Immunol 2008, 8:279–289
29. Chiang DJ, Pritchard MT, Nagy LE: Obesity, diabetes mellitus, and liver fibrosis. Am J Physiol Gastrointest Liver Physiol 2011, 300:G697–G702
30. Tacke F, Luedde T, Trautwein C: Inflammatory pathways in liver homeostasis and liver injury. Clin Rev Allergy Immunol 2009, 36:4–12
31. Hodges NJ, Innocent N, Dhanda S, Graham M: Cellular protection from oxidative DNA damage by over-expression of the novel globin cytoglobin in vitro. Mutagenesis 2008, 23:293–298
32. Fordel E, Thijs L, Martinet W, Lenjou M, Laufs T, Van Bockstaele D, Moens L, Dewilde S: Neuroglobin and cytoglobin overexpression protects human SH-SY5Y neuroblastoma cells against oxidative stress-induced cell death. Neurosci Lett 2006, 410:146–151
33. Fordel E, Thijs L, Martinet W, Schrijvers D, Moens L, Dewilde S: Anoxia or oxygen and glucose deprivation in SH-SY5Y cells: a step closer to the unraveling of neuroglobin and cytoglobin functions. Gene 2007, 398:114–122
34. Xu R, Harrison PM, Chen M, Li L, Tsui TY, Fung PC, Cheung PT, Wang G, Li H, Diao Y, Krissansen GW, Xu S, Farzaneh F: Cytoglobin overexpression protects against damage-induced fibrosis. Mol Ther 2006, 13:1093–1100
35. Halligan KE, Jourd'heuil FL, Jourd'heuil D: Cytoglobin is expressed in the vasculature and regulates cell respiration and proliferation via nitric oxide dioxygenation. J Biol Chem 2009, 284:8539–8547
36. Friedman SL: Mechanisms of hepatic fibrogenesis. Gastroenterology 2008, 134:1655–1669
37. Mimura I, Nangaku M, Nishi H, Inagi R, Tanaka T, Fujita T: Cytoglobin, a novel globin, plays an antifibrotic role in the kidney. Am J Physiol Renal Physiol 2010, 299:F1120–F1133